On the Thermal Conductivity Assessment of Oil-Based Hybrid Nanofluids using Extended Kalman Filter integrated with feed-forward neural network

Article *in* International Journal of Heat and Mass Transfer · February 2021

DOI: 10.1016/j.ijheatmasstransfer.2021.121159

CITATIONS
0

READS
115

6 authors, including:

Mehdi Jamei
Assistant Professor, Shahid Chamran university (Technology Campus of Shohada…
26 PUBLICATIONS **96** CITATIONS
SEE PROFILE

Ismail Olumegbon
Elizade University
7 PUBLICATIONS **31** CITATIONS
SEE PROFILE

Masoud Karbasi
University of Zanjan
28 PUBLICATIONS **142** CITATIONS
SEE PROFILE

Iman Ahmadianfar
Behbahan Khatam Alanbia University of Technology
44 PUBLICATIONS **259** CITATIONS
SEE PROFILE

Contents lists available at ScienceDirect

International Journal of Heat and Mass Transfer

journal homepage: http://ees.elsevier.com

On the Thermal Conductivity Assessment of Oil-Based Hybrid Nanofluids using Extended Kalman Filter integrated with feed-forward neural network

Mehdi Jamei [a,*], Ismail Adewale Olumegbon [b], Masoud Karbasi [c], Iman Ahmadianfar [d], Amin Asadi [e,*], Mehdi Mosharaf-Dehkordi [f]

[a] Faculty of Engineering, Shohadaye Hoveizeh University of Technology, Dasht-e Azadegan, Susangerd, Iran.
[b] Dep. of Physical and Chemical Sciences, Elizade University, Ondo State, Nigeria
[c] Water Engineering Department, Faculty of Agriculture, University of Zanjan, Zanjan,
[d] Dep. of Civil Engineering, Behbahan Khatam Alanbia University of Technology, Behbahan, Iran
[e] Independent Researcher, Las Vegas, Nevada, USA
[f] Dep. of Mechanical Engineering, Faculty of Engineering, University of Isfahan, Isfahan, Iran

ARTICLE INFO

Article history:
Available online xxx

Keywords
Nanofluids
thermal conductivity
oil-based hybrid nanofluids
Kalman filter
response surface methodology

ABSTRACT

Regarding their ability to enhance conventional thermal oils' thermophysical properties, oil-based hybrid nanofluids have recently been widely investigated by researchers, especially on lubrication and cooling application in the automotive industry. Thermal conductivity is one of the most crucial thermophysical properties of oil-based hybrid nanofluids, which has been studied in a minimal case of studies on the specific types of them. In this research, for the first time, a comprehensive data-intelligence analysis performed on 400 gathered data points of various types of oil-based hybrid nanofluids using a novel hybrid machine learning approach; the Extended Kalman Filter-Neural network (EKF-ANN). The genetic programming (GP) and response surface methodology (RSM) approaches were examined to appraise the main paradigm. In this research, the best subset regression analysis, as a novel feature selection scheme, was provided for finding the best input parameter among all existing predictive variables (the volume fraction, temperature, thermal conductivity of the base fluid, mean diameter, and bulk density of nanoparticles). The provided models were examined using several statistical metrics, graphical tools and trends, and sensitivity analysis. The results assessment indicated that the EKF-ANN in terms of (R = 0.9738, RMSE = 0.0071 W/m.K, and KGE = 0.9630) validation phase outperformed the RSM (R = 0.9671, RMSE = 0.0079 W/m.K, and KGE = 0.9593) and GP (R = 0.9465, RMSE = 0.010 W/m.K, and KGE = 0.9273), for accurate estimation of the thermal conductivity of oil-based hybrid nanofluids.

Nomenclature

C^*
Mallows Coefficient
D_p
Particle diameter, nm
k_{Base}
Thermal conductivity of base fluid (W/m.K)
k_{nf}
Thermal conductivity of nanofluid (W/m.K
k_p
Thermal conductivity of nanoparticle (W/m.K)
I_A
Index of agreement
m
Mass (gr)
P_c
Pearson correlation coefficient
R
Correlation coefficient
StD
Standard deviation
T
Temperature, (K)

Greek

ϕ
Nanoparticle volume fraction (%)
ρ_{nf}
Bulk fluid density, gr/cm3
ρ_{np}

Abbreviations: ASRE, Absolute standardized relative error; ANN, Artificial neural networks; AIC, Akaike's information criterion; EG, Ethylene glycol; EKF-ANN, Extended Kalman Filter-Neural network; GP, Genetic programming; KGE, Mean Square Root Error; LMI, Legates-McCabe's Index; MAPE, Mean absolute percentage error; MR, Multiple regression; PC, Amemiya's Prediction Criterion; *RSS*, Residual sum of squares; RMSE, Root mean square error (W/m.K); RD, Relative Error; RSM, Response surface methodology; SR, Standard residual.

* **Corresponding author**:
E-mail addresses: M.jamei@shhut.ac.ir (M. Jamei); Aminasadi64@gmail.com (A. Asadi)

https://doi.org/10.1016/j.ijheatmasstransfer.2021.121159
0017-9310/

ρ_{np}
Density of the nanoparticles, gr/cm3
ρ_{bf}
Density of the base fluid, gr/cm3
κ
Thermal conductivity (W/m.K)

Subscripts

bf
Base fluid
i
Nanoparticle ID
nf
Nanofluid
np
Nanoparticle
p
particles

1. Introduction

The advent of nanofluids, as a suspension of nano-sized materials into different working fluids, resulting in improved thermophysical properties, was a real breakthrough in heat transfer applications. After the pioneering study on thermophysical properties of a nanofluid by Choi et al. [1], many researchers conducted different researches on various properties [2–5] and applications of nanofluids [6–9]. Moreover, due to nanofluids' importance in heat transfer applications, various review papers have been published, summarized the published literature in different aspects of nanofluids [10–15].

Hybrid nanofluids result from the dispersion of two or more different nanomaterials combinations in a base fluid or base fluids [16]. They are generally preferred for heat transfer applications because they are characterized by higher thermal conductivity relative to the regular nanofluids [17]. Another idea behind combining nanomaterials to form a hybrid nanofluid is to allow for the synergizing of the individual nanomaterials' physio-chemical properties. Thereby giving rise to a nanofluid with improved thermal conductivity and rheological properties compared to their individual thermal conductivity [18]. The significant enhancement in hybrid nanofluids' thermal conductivity has made it imperative for use in different industrial applications. Heat transfer devices and applications, such as heat pipes [19,20], solar collectors [21,22], and so forth, require improved thermal properties for efficient transfer of heat. Spherical silica/MWCNT hybrid nanofluid showed improved performance as a better fluid in drilling operations relative to mono nanofluids [23,24]. In addition, hybrid nanofluids have been employed in power generation [25], solar thermal collectors [26], and outer-flow heat exchanger [27].

Thermal conductivity is a crucial thermophysical property that governs heat transfer rate in materials like hybrid nanofluids. As the thermal conductivity increases, the hybrid nanofluid's thermal efficiency will be increased owing to the associated convectional currents between the nanomaterials and the base fluids [28]. Many studies on the thermal conductivity of hybrid nanofluids reported an enhancement in the thermal conductivity compared to mono nanofluids [29–33]. Such enhancement can be affected by several underlying factors; the mixture or composite's synergistic effect, the nanofluid's stability, and the degree of dispersion of the base fluid. However, a few studies [23,34] recorded a reduction in hybrid nanofluids' thermal conductivity and alluded the reduction to the underlying incompatibility issues of the combining nanomaterials. In another instance, the low stability of the hybrid nanofluid caused by the synthesis method resulted in a decrease in the hybrid nanofluid [35].

Experimental investigation of hybrid nanofluids revealed that the thermal conductivity depends on properties such as the nanoparticles' size and shape [36], pH of the nanofluid, base fluid type, and the nanoparticles' volume concentration, temperature, to mention but a few [37–39]. An increase in temperature raises the kinetic energy of the hybrid nanomaterials, which causes the collision rate to increase and increase thermal conductivity [40–45]. An experimental investigation involving water-based f-MWCNT/f-HEG [46], DI water-based Ag/HEG [47], EG based Al/Zn, and water-based Al_2O_3/Cu [33] showed enhancement in thermal conductivity as the volume fraction and temperature increases. Furthermore, the choice of base fluid for a hybrid nanofluid formation influences the thermal conductivity. For instance, water-based hybrid nanofluid produces a higher thermal conductivity than ethylene glycol-based hybrid nanofluid [48–50]. The shape of hybrid nanomaterials can affect the value of the thermal conductivity. Cylindrical-shaped nanomaterial, such as CNT, produces a higher thermal conductivity than spherical-shaped nanomaterial when dispersed in similar base fluids [51,52]. Moreover, the size of the combining nanomaterials varies inversely with the thermal conductivity. Thus, small-sized nanomaterials will possess higher thermal conductivity than large-sized ones due to their increased collision rate. The study on EG-based Al/Zn reported a nonlinear increase in thermal conductivity as the composite or crystallite size decreases [53]. A highlight of studies on oil-based hybrid nanofluid showing the dependence of thermal conductivity on some of these factors is presented in table 1.

2. Theoretical background and data-driven based literature review

Previously, novel attempts were made by Maxwell [61], Hamiton and Crosser [62], Jang and Choi [63], Bhattechaya et al. [64], and Mahmid et al. [65,66] to evolve a general numerical model for calculating the thermal conductivity of nanofluids. However, none of such efforts could give an accurate estimation of the thermal conductivity of specific nanofluids. Researchers have developed empirical correlations specific to different classes of nanofluids in the absence of a generalized numerical model. A few of such correlations on the thermal conductivity (K_{nf}) of oil-based hybrid nanofluid as a function of volume fraction (ϕ) and temperature (T) were developed. Table 2 addresses some of these correlations for estimating the thermal conductivity of oil-based, EG&Water based hybrid nanofluids. Moreover, the correlations proposed by Pak and Cho [67] and Mintsa et al. [61] have been examined to validate other thermal conductivity measurements or estimates for hybrid nanofluids.

So far, there is no generally applicable numerical model or correlation for estimating hybrid nanofluids' thermal conductivity. Besides, the inherent inaccuracies become apparent as a result of the underlying anomalous nature of nanofluids. These inadequacies pave the way for the emergence of the machine learning (ML) approach, considering their robust predictive and generalization capabilities. The application of ML methodologies in developing highly accurate models for estimating nanofluids' thermophysical properties is actively on-

Table 1
Experimental studies on the thermal conductivity of oil-based hybrid nanofluids.

Nanomaterial	Base fluid	Thermal conductivity improvement	Reference
Al_2O_3-MWCNT	Thermal oil	45% increase at T = 50C and ϕ = 1.5%	Asadi et al. [54]
MgO-MWCNT	Engine Oil	65% increase at 50C and ϕ = 2%	Asadi et al. [55]
Mg (OH)2-MWCNT	Engine Oil	50% increase at 60C and ϕ = 2%	Asadi et al. [56]
SiC-TiO_2	Diathermic oil	8.39% increase at T = 43C and ϕ = 1%	Wei et al. [29]
Cu-Zn	Vegetable oil	130% increase at 60C and ϕ = 0.5%	Mechiri et al. [57]
Cu-Zn	Vegetable oil, Paraffin oil, SAE oil	67% increase at 30 C and ϕ = 0.5%	Kumar et al. [40]
SiO_2-Graphene	Naphthenic Mineral oil	80% increase at 100 C, ϕ = 0.04%	Qing et al. [58]
Silica-Ag	Transformer oil	15% increase at (ϕ = 0.6%) in Ag and (ϕ = 0.07%) in Silica	Botha et al. [59]
WO3-Ag	Transformer oil	41% increase at T = 100C and ϕ = 4%	Aberoumand et al. [60]

ϕ - Volume concentration, T-Temperature

Table 2
The experimental based correlation for oil-based hybrid nanofluids to validate the provided AI models

Model	Nanoparticles	Formula	Base fluid
Soltani et al.[68]	WO3-MWCNTs	$\frac{k_{nf}}{k_{Base}} = \frac{0.914(1.3974\phi^{0.3681})(0.00777T^{0.7787})}{Exp((-310.0683\phi^2)(T^{-1.9772}))}$	Engine Oil
Mechiri et. al. [57]	Cu-Zn	$k_{eff} = 0.7054 + 0.009896T + 0.8717\phi - 6.479\times10^{-5}T^2 + 0.09749T\phi - 4.714\phi^2 - 0.0002718T^2\phi - 0.1174T\phi^2 + 10.09\phi^3$	Vegetable oil
Asadi et al.[54]	Al2O3-MWCNT	$k_{nf} = 0.1534 + 0.00026T + 1.1193\phi$	Oil
Asadi et al.[55]	MgO-MWCNT	$k_{nf} = 0.162 + 0.00051T + 0.691\phi$	Oil
Asadi et al.[56]	Mg (OH)2-MWCNT	$k_{nf} = 0.159 + 0.003T + 1.1112\phi$	Engine Oil
Pak and Cho [67]	Metal oxides	$k_{nf} = k_{Base}(1 + 7.47\phi)$	Water
Toghraie et al.[69]	ZnO–TiO_2	$\frac{k_{nf}}{k_{bf}} = 1 + 0.004503\phi^{0.8717}T^{0.7972}$	EG
Harandi et al. [70]	F-MWCNTs–Fe_3O_4	$\frac{k_{nf}}{k_{bf}} = 1 + 0.0162\phi^{0.7038}T^{0.6009}$	EG
Esfahani et al.[71]	ZnO-Ag	$\frac{k_{nf}}{k_{bf}} = 1 + 0.0008794\varphi^{0.5899}T^{1.345}$	Water
Mintsa et al.[72]	Al_2O_3/Cuo/SiO_2/ZnO-	$\frac{k_{nf}}{k_{bf}} = 1.72\phi + 1.0$	Water

going, given its proven accuracy. ML models have been constructed to estimate viscosity [73–77], specific heat capacity [78–81], and even thermal conductivity [82–87] using various learning algorithm such as artificial neural networks (ANN) [75,88], support vector regression (SVR) [78,89], genetic programming (GEP) [82], to mention but a few. ML application in nanofluids studies involves using the nanomaterials' physical and chemical properties and base fluids as model inputs and the thermophysical property under investigation as the target variable. Over the years, a few ML studies have been dedicated to estimating hybrid nanofluids' thermal conductivity. A historical highlight of such research efforts has been presented in Table 3.

Table 3
The highlight of machine learning studies for predicting the thermal conductivity of hybrid nanofluids.

Nanoparticles	Base fluid	Model inputs	Methodology	Ref.
Cu-Zn	Water	ϕ, T	ANFIS	Balla et al. [90]
CuO-SWCNT	EG-water	ϕ, T	MLP	Rostamian et al. [91]
MgO-MWCNT	EG	ϕ, T	ANN	Vafaei et al. [92]
SWCNT-ZnO	EG-water	ϕ, T	ANN	Esfe et al. [93]
ZnO-MWCNT	EG-water	ϕ, T	MLP	Esfe et al. [94]
SWCNT-Al_2O_3	EG	ϕ, T	ANN	Esfe et al. [95]
MWCNT-SiO_2	EG	ϕ, T	MLP	Esfe et al. [96]
CNT-Fe3O4	Water	ϕ, T	MLP	Shahsavar et al. [97]
SWCNT-MgO	EG	ϕ, T	ANN	Esfe et al. [98]
Al2O3-SiO_2	Water	ϕ, T	MLP	Kannaiyan et al. [99]
DWCNT-SiO_2	EG	ϕ, T	MLP	Esfe et al. [100]
Cu-Al_2O_3	Water		LSM	Usman et al.[101]
Various nanoparticles		ϕ, T	ANN	Adun et al.[86]
Various nanoparticles	EG	$\phi, T, D_p, \rho, k_{Base}$	GEP, MT, MLR	Jamei et al. [82]
Various nanoparticles	W-EG	$\phi, T, D_p, \rho, k_p, k_{Base}, \beta$	LWLR,GLP, GEP	Pourrajab et al. [83]

ANFIS-Adaptive Neuro-Fuzzy Interference System, MLP-Multilayer Perceptron, GEP- Genetic programming, MT- Model tree, MLR- Multilinear regression

3. Dataset description and best feature selection procedure

For the development of data-driven models in this research, seven influential variables including volume fraction of nanoparticles (ϕ), temperature (T), the average diameter of nanoparticles for each set of particles (D_{p1}andD_{p2}), the thermal conductivity of the base fluid (k_{Base}), and the density of each nanofluid (i.e.,$\rho_1$and ρ_2) were collected from 6 references as shown in Table 4.

The descriptive statistics of the predictive variables are summarized in Table 5. The statistical assessment of the datasets showed the maximum/minimum skewness (-2.144) and kurtosis (2.611) values are relatively in the allowable range ([-2.2, 2.2]) [104,105], which confirms the competence of the data to provide the predictive models. Furthermore, the Shapiro-Wilk normality test [106] indicated that none of the parameters do satisfy the normality distribution. It is noteworthy that the nanoparticle with the greater density (ρ_1) is assigned subscript 1, and that of the lighter nanoparticle (ρ_2) is assigned subscript 2.

To develop a robust and computationally efficient AI-based model, one needs to utilize a proper feature selection procedure that provides a set of the most critical independent parameters. In fact, a well-suited selection procedure reduces the computational costs of the model by decreasing the number of independent variables [107,108]. To determine the optimal set of independent variables, the best subset regression algorithm [109] can be employed to extract the best subsets regression fitting all possible models. Based on three objective criteria, including the adjusted R-squared, Mallow's coefficient [94], Akaike's information criterion [110], and Amemiya's Prediction Criterion [111], the most appropriate fitting models are selected [94]. These criteria are briefly described in the following.

Mallow's coefficient

Based on the total number of k parameters and mean squared error (MSE_m(, the Mallow coefficient (C^*) is defined as [94]:

Table 4
experimental datasets characteristics used for designing the data-driven models for prediction of the thermal conductivity of oil-based hybrid nanofluids.

References	Number of Data	Nanoparticles	Base fluid
[54]	42	Al_2O_3-MWCNT	Pure Oil
[102]	54	TiO_2-SiC	Pure diathermic Oil
[56]	56	Mg(OH)2-MWCNT	Engine Oil
[68]	55	WO3- MWCNTs	Engine Oil
[103]	128	TiO2, SiO2, Al_2O_3-MWCNTs	Transformer Oil
[55]	65	MgO- MWCNTs	Engine Oil

Table 5
The descriptive statistics of predictive variables and targets.

Metrics	ϕ	T	D_{p1}	ρ_1	D_{p2}	ρ_2	k_{Base}	k_{nf}
Minimum	0.000	15.000	10.000	0.200	15.000	0.110	0.101	0.106
Maximum	2.000	75.000	65.000	7.160	30.000	2.100	0.194	0.228
Mean	0.396	40.920	30.280	3.455	23.180	1.831	0.132	0.149
Std. Deviation	0.486	15.490	18.320	1.931	5.969	0.681	0.025	0.031
Range	2.000	60.000	55.000	6.960	15.000	1.990	0.093	0.121
Skewness	1.419	0.414	0.533	0.293	-0.402	-2.144	0.920	0.250
Kurtosis	1.406	-0.579	-0.947	0.011	-1.395	2.611	0.585	-1.238
Shapiro-Wilk test for normal distribution								
W	0.793	0.959	0.873	0.881	0.774	0.404	0.859	0.916
P value	<0.0001	<0.0001	<0.0001	<0.0001	<0.0001	<0.0001	<0.0001	<0.0001
Is normality test passed (alpha = 0.05)?	No	No	No	No	No	No	No	No

$$C^* = \frac{RSS_k}{MSE_m} + 2k - N,\ m>k \tag{1}$$

Where RSS_k stands for the residual sum of squares associated with the regression model, and N represents the total number of data points.

Akaike's information criterion

Akaike's information criterion (AIC) is an estimator, which can be used to determine the relative quality of different statistical models for a given dataset. This means that AIC can be seen as a model selection tool. As a criterion, the AIC parameter associated with each desirable model is defined as [110]:

$$AIC = 2p + n\cdot \ln\left(\frac{1}{N}\sum_{i=1}^{n}\hat{e}_i^2\right) \tag{2}$$

Where N and P are the number of samples (data points) and the number of parameters in the model, respectively. Besides, the term $\sum_{i=1}^{n}\hat{e}_i^2$ is the residual sum of squares in which $\hat{e}_i$ stands for i-th RESS residual. Once AIC parameter is calculated for all models, the model associated with the minimum AIC value is chosen as the best one [34].

Amemiya's Prediction Criterion (PC)

Amemiya's Prediction Criterion is expressed by the following relation [111]:

$$PC = \frac{1}{(N-p)}\sum_{i=1}^{n}\hat{e}_i^2\left(1+\frac{p}{N}\right) \tag{3}$$

Where P is the number of parameters in the model, N is the number of samples, and $\hat{e}_i$ represents i-th RESS residual. Like AIC, a minimum value of PC is desirable, which can be used to select the best combination set.

In this section, the mentioned criteria are used to select the best combination of the parameters representing the optimal set of independent variables. Considering the data given in Table 6 and also Fig. 1 for the highest values of R^2 and R^2-adj along with the lowest values of Mallow's factor, Akaike's AIC, and Amemiya's PC, it is observed that the two last combinations (i.e., C6 and C7) can be considered as the best choices for the optimal combination set. However, the density of a nanofluid is neglected in the combination C6, while the other nanofluid density is incorporated into the combination. Based on this point, it seems reasonable to choose the combination C7, considering the same parameters for both nanofluids, as the best combination. As a result, the optimal set of independent parameters consists of seven members, including temperature (T), the volume fraction of nanoparticles (ϕ), the average diameter of nanoparticles for each set of particles (D_{p1} and D_{p2}), the thermal conductivity of the base fluid (k_{Base}), and the density of each nanofluid (i.e., ρ_1 and ρ_2). Therefore, the thermal conductivity of oil-based hybrid nanofluid is expressed as:

$$k_{nf} = f\left(\phi, T, D_{p1}, \rho_1, D_{p2}, \rho_2, k_{Base}\right) \tag{4}$$

here, the particle volume fraction is defined as:

$$\phi = \left((m/\rho)_{np1} + (m/\rho)_{np2}\right) / \left((m/\rho)_{np1} + (m/\rho)_{np2} + (m/\rho)_{bf}\right) \tag{5}$$

Where m_{np} and m_{bf} are the total mass of the nanoparticles and base fluid, respectively. In this research, 75% (300 samples) of datasets were allocated for the training model s, and 25% of datasets were implemented for validation (testing phase).

The Pearson correlation coefficient between each independent variable and thermal conductivity is illustrated in Fig. 2. The Pearson correlation coefficient values represent that nanofluids' thermal conductivity has the most linear correlation with the volume fraction of solids ($P_c = 0.725$) and thermal conductivity of the base fluid ($P_c = 0.696$). The results shown in Fig. 2 represent that it has a more linear correlation with D_{p2} ($P_c = 0.696$) than D_{p1} ($P_c = -0.466$).

To decrease the computational costs of predicting procedure, the independent variables and also responses are normalized by using the following relation:

$$X_{nor} = \frac{X - X_{min}}{X_{max} - X_{min}} \tag{6}$$

Here, X is the primary basic value, X_{nor} is the normalized value, and subscripts min and max stand for the minimum and maximum values of the dataset incorporated into the predictive models, respectively.

Table 6
Best subsets regression results for determining the optimum input combination

Combo	No. of variables	Variables	R^2	Adjusted R^2	Mallows' C*	Akaike's AIC	Amemiya's PC
C1	1	ϕ	0.526	0.524	828.794	-3070.54	0.477
C2	2	D_{p2}, ρ_2	0.720	0.719	328.678	-3279.57	0.283
C3	3	ϕ, D_{p2}, ρ_2	0.822	0.821	67.160	-3458.40	0.181
C4	4	$\phi, D_{p2}, \rho_2, k_{Base}$	0.836	0.834	33.683	-3489.16	0.167
C5	5	$\phi, T, D_{p2}, \rho_2, k_{Base}$	0.847	0.845	8.260	-3513.92	0.157
C6	6	$\phi, T, D_{p1}, D_{p2}, \rho_2, k_{Base}$	0.848	0.8455	6.743	-3515.49	0.158
C7	7	$\phi, T, D_{p1}, \rho_1, D_{p2}, \rho_2, k_{Base}$	**0.848**	**0.84546**	**8**	**-3514.2**	**0.157**

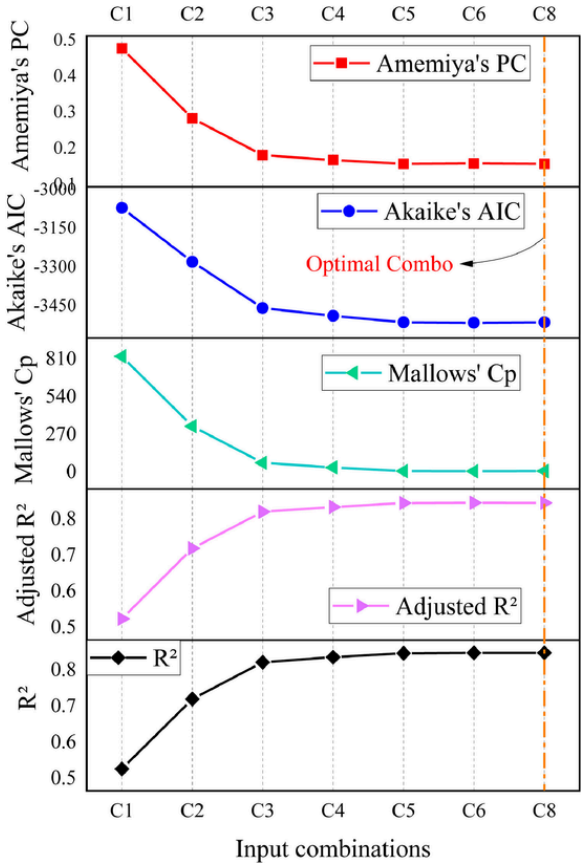

Fig. 1. The values of different selection criteria for different combination sets

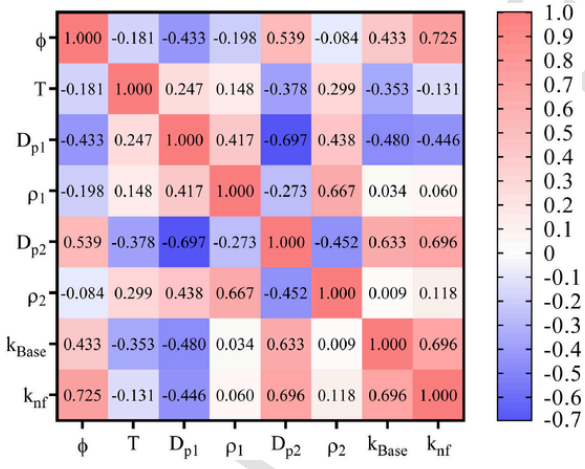

Fig. 2. The Pearson correlation coefficient between the independent input variable and thermal conductivity

4. Methodology

4.1. Artificial neural network (ANN)

Artificial neural networks are a way to approximate the functions and predict the future state of different systems. The artificial neural network structure is characterized by four traits, including the number of neurons in each layer, the type of transfer functions, the number of layers, and the training algorithm [112]. The smallest information processing unit in an artificial neural network is the neuron, which forms the artificial neural networks' core. Artificial neural networks process observational data, discover the connection between them, and transfer them into the network. Artificial neural networks are made up of a number of nodes that are the same as the neurons and the weights that connect the input neurons. The input data is multiplied by their corresponding weights, and the sum of them is input to the neurons. Each neuron has a transfer function. The input value is placed in the transfer function, and the resulting value determines the neuron's output. The transfer function can be linear or nonlinear. The most popular transfer functions are sigmoid, logistic, and hyperbolic functions [112]. The function must be finite, incremental, continuous, and derivative and must be selected based on the modeling problem. Artificial neural networks can be single-layer or multilayer. Multilayer perceptron networks are known as MLP neural networks. In general, the mathematical form of the output signal of artificial neurons can be written as follows:

$$o = h_0\left[\sum_{j=1}^{m} W_{kj}.h_h\left(\sum_{i=1}^{n} W_{ij}x_i + W_{j0}\right) + W_{k0}\right] \tag{7}$$

where x_i is the input signal W is the synaptic weight, n, m, and k respectively are the total number of neurons in the input, hidden, and output layers. The functions h_h and h_0 are transfer functions for hidden and output layers, respectively, and o is the output of the neural network. Typically, the back propagation (BP) algorithm is used to train the artificial neural network [113].

4.2. Hybridized Extended Kalman filter algorithm with Feed-Forward neural network (EKF-ANN)

Kalman filter is one of the most famous and widely used mathematical tools, which is used for statistical estimates. The classic Kalman filter solves the problem of discrete linear filtering based on a recursive method. This algorithm is implemented in two steps. In the prediction step, the Kalman filter estimates the current state of the variables under uncertainty. When the next measurement result is obtained, the previous estimate is updated with the weighted average. The algorithm is recursive and is executed immediately using new inputs and previously calculated scenarios [114].

If the relationships between the state and output variables are nonlinear, the extended Kalman filter (EKF) algorithm is used [115]. Feed-Forward neural network can be considered a nonlinear dynamic system with synaptic weights [116]. Neural network training can be equated with the problem of estimating the state of the nonlinear system. For this reason, the extended version of the Kalman filter can be used to estimate adjustable neural network parameters (weights and biases). As a result, the neural network must be formulated according to state-space concepts (similar to what is called in nonlinear dynamic systems) to obtain the best value of the parameter developed by the Kalman filter. Consider Fig.3 as a single-layered neural network used to identify the primary system. This neural network can be defined as finite-dimensional discrete-time systems with the following relations [117]:

$$W_{N_w\times 1}(k+1) = W_{N_w\times 1}(k) + n_{N_w\times 1}(k) \tag{8}$$

$$y_{n_2\times 1}(k+1) = h(w(k), x(k)) + v_{n_2\times 1}(k) \tag{9}$$

Equation (8) is the process model in which the neural network weight vector ($W(k)$) is ideally impregnated as a process state ($n(0)$) as a system state. Equation (9) expresses the measurement model to obtain the nonlinear neural network's response to the input vector ($x(k)$) and its weights. The parameter $v(k)$ is the measured noise and $h[W(k), x(k)]$ is used as the activating function to describe the model's nonlinear part. Measurement noise is considered random with zero mean and $R(0)$ covariance, and process noise is considered with zero mean and $Q(0)$ covariance [117].

The weight vector includes all the weights of the hidden layers and the neural network's output and is defined as equation 10.

$$W_{N_w\times 1} = \left[w_1, w_2, \ldots, w_{N_w}\right]^T \tag{10}$$

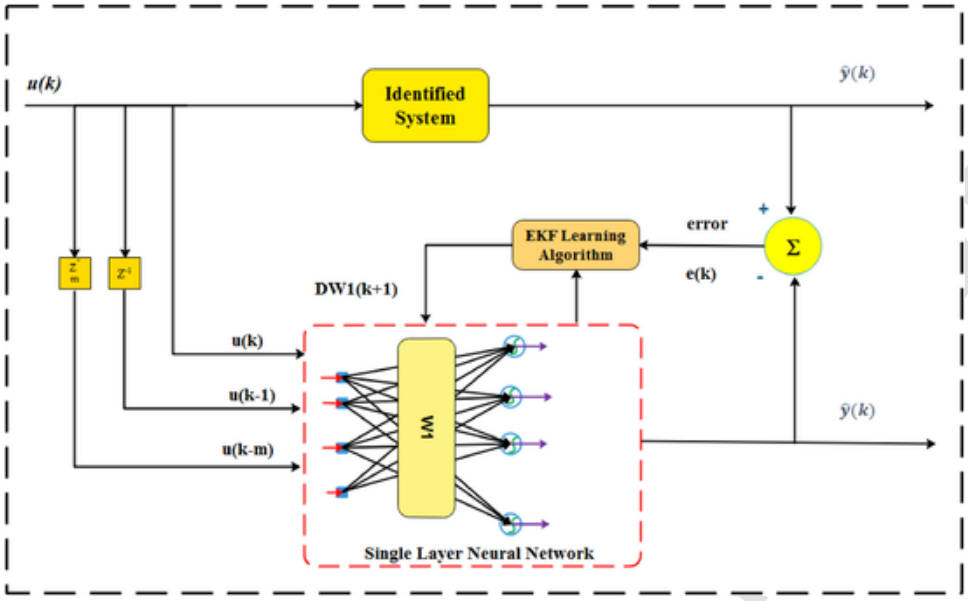

Fig. 3. Structure of a single layer neural network with extended Kalman filter training algorithm

Here, a neural network with an activating intermediate layer is considered, in which n_0, n_1, and n_2 are the number of input, intermediate, and output signals, respectively. Thus, the total number of weights is $N_w = n_1 \times n_0 + n_2 \times n_1$. The extended Kalman filter adjusts the neural network weights to minimize the mean squares of the estimation error. In summary, the weight adjustment process in the EKF method is performed according to the following recursive relations [118]:

$$A_{n_2\times n_2}(k) = \left[R_{n_2\times n_2}(k) + H^T_{n_2\times N_w}(k).P_{N_w\times N_w}(k).H_{N_w\times n_2}(k)\right]^{-1} \quad (11)$$

$$K_{N_w\times n_2}(k) = P_{N_w\times N_w}(k).H_{N_w\times n_2}(k).A_{n_2\times n_2}(k) \quad (12)$$

$$W_{N_w\times 1}(k+1) = W_{N_w\times 1}(k) + K_{N_w\times n_2}(k).e_{n_2\times 1}(k) \quad (13)$$

$$P_{N_w\times N_w}(k+1) = P_{N_w\times N_w}(k) - K_{N_w\times n_2}(k).H^T_{n_2\times N_w}(k).P_{N_w\times N_w}(k) + Q_{N_w\times N_w}(k$$

$$e_{n_2\times 1}(k) = y_{n_2\times 1}(k) + \hat{y}_{n_2\times 1}(k) \quad (15)$$

In these equations, $K(k)$ the Kalman gain matrix, the estimation error, is observed data. The neural network output, the error covariance matrix, $H(k)$ is the output derivative matrix according to weights and $A(k)$ is the normalization matrix. The derivative matrix $H(k)$ is a Jacobin matrix of neural network outputs relative to its weights, which can be calculated using the following equation [119]:

$$H_{N_w\times n_2}(k) = \left[\frac{\partial\hat{y}(k)}{\partial W_{1n_2\times 1}(k)}, \frac{\partial\hat{y}(k)}{\partial W_{2n_2\times 1}(k)}, \cdots, \frac{\partial\hat{y}(k)}{\partial W_{Nwn_2\times 1}(k)}\right]^T_{N_w\times n_2} \quad (16)$$

4.3. EKF-ANN implementation algorithm

The stages of the ANN-EKF algorithm can be summarized as follows:

Step 1: Obtain the output vector of the neural network in step k using Eqs (8) and (9) ($\hat{y}(k)$)
Step 2: Obtain the output derivative matrix relative to the weights using Eq (16) ($H(k)$).
Step 3: Calculate the estimation error vector using Eq (15) ($e(k)$).
Step 4: Calculate the Kalman filter gain with Eq (12) ($K(k)$).
Step 5: Obtain the error covariance matrix and adjust the weights for step k + 1 using Eq (13) and (14) ($W(k+1)$ and $P(k+1)$).

The initial value of the weights is selected randomly with a zero-mean value and a uniform or normal distribution. The initial error covariance matrix can also be selected as:

$$P(0) = \varepsilon^{-1} I \quad (17)$$

Where I is the identity matrix and $\varepsilon = [0.001, 0.01]$. the measurement noise covariance matrix is considered as:

$$R(k) = \eta^{-1}(k) I \quad (18)$$

Where the learning rate $\eta(k)$ and its value is in the range of $[10^{-2}, 10^{-4}]$. The process noise covariance matrix is considered as:

$$Q(k) = q(k) I \quad (19)$$

Which $q(k)$ is initially selected to be 0.1 and decreases overtime to reach approximately10^{-6}. This decreasing trend of the coefficient $q(k)$ causes faster convergence, and its non-zero value prevents the divergence of the error covariance matrix [120].

4.4. Genetic programming (GP)

The genetic programming paradigm is an evolutionary computational intelligence technique built on the foundation of the random biologically inspired algorithm, which is characterized by its reliance and freedom in explaining complex processes using logical functions and mathematical expressions. Usually, GP utilizes a tree structural representation for decision features to create the solution in an expression formation composed of elements like a tree and terminal nodes. In such formalism, the tree node symbolizes function, and the terminal node can represent an operand. In GP, numerical and categorical decision features are labeled as a terminal set, while arithmetic symbols (-, +, ×, ÷), logical operators (e.g., if-then-else), and mathematical functions are described as function set. A demonstration of GP methodology is highlighted in Fig. 4. The existing mathematic operations in Fig. 4 (upper panel) are "*" and "-"and which represents the expression of "A-6C" for tree structure on the left side of and "$A \times 6C$" on the right side, respectively. The procedural operation of a GP is enumerated as follows:

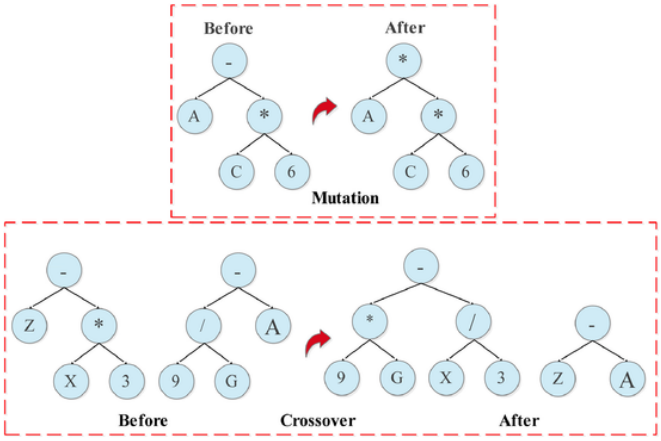

Fig. 4. The example of mutation (Upper panel) and crossover (Lower panel) procedure in GP model

Step 1: a randomized system of trees is initialized, and the associated objective functions of the individual trees are evaluated.
Step 2: The trees' objective function is compared and the optimal objective functions are selected by using the roulette wheel or tournament methods.
Step 3: the set of operators known as the crossover and mutation operators are employed to reproduce the next set of trees.
Step 4: the recursive process of tree reproduction is continued until it is maximal enough and the process is terminated. Otherwise, the iteration begins again in step 2.

The crossover operator's role is to join two trees as a unit and subsequently use the unit to generate another two new unit sets. Upon generating a new unit, elemental change in the individual unit is produced using the mutation operator. Fig. 4 highlights the application of the mutation and crossover operator on one and two units, respectively.

4.5. Response surface methodology (RSM)

RSM is an aggregation of statistical approach and mathematical technique for obtaining simultaneous solutions of multivariate equations using data collected from a series of designed experimental observations. It measures the connection between input factors (say three) and one or more responses and determines the appropriate conditions for which the input factors will yield an optimal response. A hypothesized mathematical model in RSM, usually a second-order polynomial. Equation (17) is fitted to the data under the selected, designed observations.

$$Y = \theta_0 + \sum_{i=1}^{K}\theta_i x_i + \sum_{i=1}^{K}\sum_{j=1,j\neq i}^{K}\theta_{ij}x_i x_j + \sum_{i=1}^{K}\theta_{ii}{x_i}^2 + \varepsilon \tag{20}$$

Where Y is the predicted value of the target, θ_0 is a constant, θ_i, θ_{ii} and θ_{ij} are linear, quadratic, and cross product terms, respectively [121].

4.6. Evaluation indices of models

In order to evaluate the accuracy of the models and compare them with each other, Correlation coefficient (R), Root mean square error (RMSE), Relative absolute error (RAE), and Willmott's agreement Index (IA) statistical criteria were used [122]. Besides efficient multi-objective criteria, Kling-Gupta efficiency (KGE) [123] was examined to specify the well-established approaches better. KGE is decomposed into the correlation coefficient, variability (standard deviation), and the models' mean magnitude.

$$R = \frac{\sum_{i=1}^{N}\left(k_{nf}p_i - \overline{k_{nf}p}\right).\left(k_{nf}o_i - \overline{k_{nf}o}\right)}{\sqrt{\sum_{i=1}^{N}\left(k_{nf}p_i - \overline{k_{nf}p}\right)^2 \sum_{i}^{N}\left(k_{nf}o_i - \overline{k_{nf}o}\right)^2}} \tag{21}$$

$$RMSE = \left(\frac{1}{N}\sum_{i=1}^{N}\left(k_{nf}o_i - k_{nf}p_i\right)^2\right)^{0.5} \tag{22}$$

$$RAE = \frac{\sum_{i=1}^{N}\left|k_{nf}o_i - k_{nf}p_i\right|}{\sum_{i=1}^{N}\left|k_{nf}o_i - \overline{k_{nf}o}\right|} \tag{23}$$

$$KGE = 1 - \sqrt{(R-1)^2 + \left(StD_p/StD_o - 1\right)^2 + \left(\overline{k_{nf}p}/\overline{k_{nf}o} - 1\right)^2} \tag{24}$$

$$I_A = 1 - \frac{\sum_{i}^{N}\left(k_{nf}o_i - k_{nf}p_i\right)^2}{\sum_{i=1}^{N}\left(\left|\left(k_{nf}o_i - \overline{k_{nf}o}\right)\right| + \left|\left(k_{nf}o_i - \overline{k_{nf}o}\right)\right|\right)^2},\ 0<I_A \leq 1 \tag{25}$$

where $k_{nf}o_i$ is observed value, $k_{nf}p_i$is the predicted value, $\overline{k_{nf}o}$and $\overline{k_{nf}p}$ are the average values of observed and predicted data, $StD_o$and StD_p are standard deviation values of observed and predicted data, and N is the number of data points. If the RMSE, MAE, and RAE are close to zero and R, KGE and I_A are close to unity; the model achieves better performance.

5. Model formulation

In this study, three robust data-driven models, including EKF-ANN, GP, and RSM approaches, were developed to predict oil-based hybrid nanofluids' thermal conductivity. All provided models were designed in Matlab 2018b, and modeling was performed on an Intel, core i7 core CPU Intel with frequency 3.2 GHz and 8 GB RAM computer. The EKF, as the main novel predictive model, has two crucial parameters comprising the neuron and epoch numbers achieved by a trial and error procedure. Various attempts at performing the EKF-ANN model demonstrated that the optimal neuron number and epoch value was obtained equal to 2 and 300, respectively. Also, the characteristics of GP based on the simple mathematical operators (i.e., +, -,×, /, and) were listed in Table 7. RSM, as one the most common data-driven models based on a quadratic approximation, yields a reasonable estimation of various aspects of nanofluids in computational heat transfer engineering applications. The result of the RSM approach is reported in Table 8, which provides the optimal relationship with quadratic approximation. The process of the thermal conductivity of oil-based hybrid nanofluids modeling using three adopted data-driven models is exhibited in Fig. 5.

Table 7
The GP method characteristics

Description of parameter	Parameters specification
Function set	+, −, ×, /,
Population size	400
Stop criteria	Maximum number of iterations (200)
Maximum gene numbers	4
Selection	tournament
Tournament size	8
Maximal tree depth	5
Mutation probability	0.15
Crossover probability	0.85
Crossover operators	Subtree
Mutation operators	Gaussian

Table 8
the estimated Coefficients in RSM approaches using a quadratic approximation

inputs	Estimate	SE	tStat	pValue
(Intercept)	-0.7561	0.1431	-5.2845	0.0000
x1	0.0538	0.0116	4.6451	0.0000
x2	-0.0001	0.0002	-0.6017	0.5478
x3	0.0080	0.0019	4.2823	0.0000
x4	0.0125	0.0097	1.2855	0.1997
x5	0.0588	0.0095	6.2233	0.0000
x6	0.0228	0.0068	3.3469	0.0009
x7	2.3999	0.5592	4.2919	0.0000
x1:x2	0.0005	0.0001	4.4922	0.0000
x1:x3	0.0004	0.0002	2.1695	0.0309
x1:x6	0.0100	0.0028	3.5985	0.0004
x1:x7	-0.3476	0.0642	-5.4138	0.0000
x2:x3	0.0000	0.0000	-2.2959	0.0224
x2:x5	0.0000	0.0000	2.2212	0.0271
x3:x7	-0.0727	0.0165	-4.3940	0.0000
x4:x7	-0.2820	0.1225	-2.3024	0.0220
x1^2	-0.0143	0.0025	-5.6525	0.0000
x4^2	0.0026	0.0010	2.6967	0.0074

6. Application results and discussion

As proven before, best subset regression analysis proved that the best input combination is including solid volume fraction (ϕ), temperature (T), the thermal conductivity of the base fluid (k_{Base}), mean diameter (D_{p1} and D_{p2}), and bulk density ($\rho_1$andρ_2) of nanoparticles. The provided predictive models were performed several times to converge to stable and reliable results. Table 9 demonstrated the "goodness of fit" measures for training, testing, and all datasets to the prediction of k_{nf}. The results indicated that EKF-ANN in terms of (R = 0.9728, RMSE = 0.0071 W/m.K, KGE = 0.961) in training and (R = 0.9764, RMSE = 0.0069 W/m.K, KGE = 0.9989) testing, respectively was identified as the superior model in comparison with GP and RSM approaches for estimating the k_{nf}. Besides, an accurate quantitative comparison on all datasets indicated that the EKF-ANN on account of higher correlation coefficient (R = 0.9738,) and KPG (0.9630) as well as the lowest error metrics (RMSE = 0.0071 W/m.K, MAPE = 2.4751%) was outperformed the RSM (R = 0.9671, KGE = 0.9593, RMSE = 0.0079 W/m.K, MAPE = 2.9219%) and GP (R = 0.9465, KGE = 0.9273, RMSE = 0.0100 W/m.K, MAPE = 4.6257%). The RSM was standing on the second rank and had a better performance versus the GP model.

As the graphical evaluation, Fig. 6 indicated the distribution density function (Left) and scatter plots (Right) of thermal conductivity of oil-based nanofluids in the training and testing phase for all three data-driven models. Fig. 6 (Left) indicated that EKF-ANN and RSM have closer distribution to measured values than the GP model. However, it this crystal clear that RSM values showed fairly overfitting in both training and testing modes. Further-

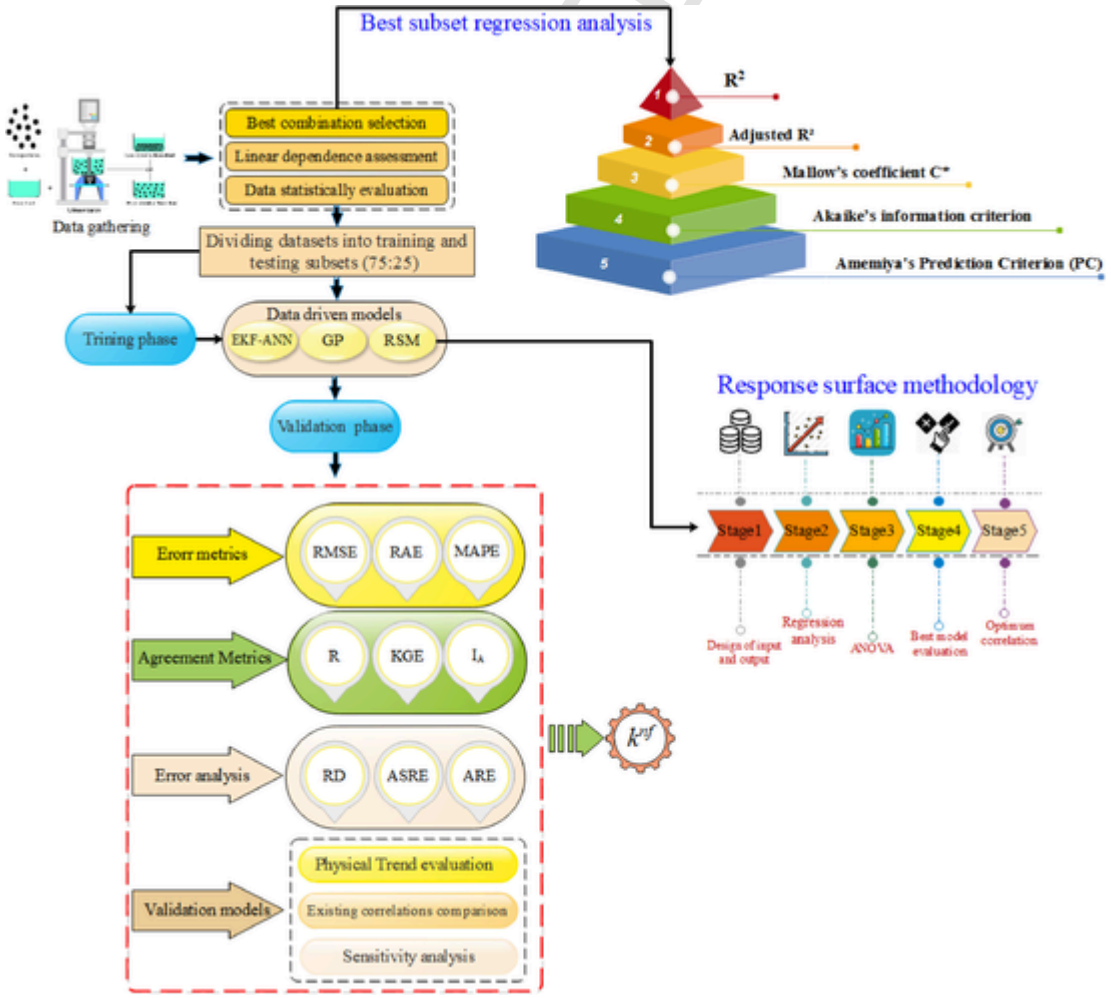

Fig. 5. Road map of thermal conductivity of oil-based hybrid nanofluids

Table 9
The statistical evaluation of all predictive models for training, testing, and all data sets.

	Metrics	EKF-ANN	RSM	GP
Train	R	0.9728	0.9657	0.9430
	RMSE	0.0071	0.0080	0.0103
	MAPE	2.4947	2.9052	4.7063
	RAE	0.1404	0.1629	0.2575
	KGE	0.9610	0.9515	0.9194
	I_A	0.9861	0.9824	0.9700
Test	R	0.9764	0.9720	0.9560
	RMSE	0.0069	0.0077	0.0094
	MAPE	2.4165	2.9722	4.3838
	RAE	0.1337	0.1623	0.2396
	KGE	0.9989	0.9703	0.9475
	I_A	0.9880	0.9855	0.9775
All	R	0.9738	0.9671	0.9465
	RMSE	0.0071	0.0079	0.0100
	MAPE	2.4751	2.9219	4.6257
	RAE	0.1386	0.1627	0.2529
	KGE	0.9630	0.9593	0.9273
	I_A	0.9866	0.9833	0.9721

more, the scatter plots confirmed the superiority of the KFE-ANN model compared to RSM and GP, regarding closer compliance and least dispersion relative to the X-Y line. The best predictive performance of KFE-ANN and RSM occurred in the range of ($0.15 \le k_{nf} \le 0.23$) whereas GP results exceed the ±20% error line at the plot's higher zones.

In the next validation of models, a comprehensive error analysis was conducted based on a percentage of relative error (PRE %), standardized residual error (ASRE), and frequency cumulative absolute percentage of relative error (RE) and absolute ASRE to more appraising the developed predictive schemes (Figs. 7 and 8). The left column of Fig. 6 depicted the PRE contours of the developed models versus ϕ and k_{Base} variations. Clearly can be seen that EKF-ANN ($-40.8\% \le PRE \le 11\%$) and RSM models ($-38.4\% \le PRE \le 13.8\%$) by least range of PRE have better performance in predicting the thermal conductivity of oil-based hybrid nanofluids. Moreover, EKF-ANN and RSM models for the high value of k_{Base} and low value of ϕ maybe trapped on underestimation. Most understudy domains have acceptable PRE values (>5%) and yield to appropriate results.

Fig.6 the violin plots of distribution function (Left) and scatter plot (Right) of measured and predicted thermal conductivity of oil-based hybrid nanofluids

The right column of Fig. 7 illustrated the ASRE distribution. The quantitative measurement evidenced that the EKF-ANN approach by the range of ($-1.67 \le ASRE \le 0.7$, error band: 2.37) was ranked as the best model and yielded the promising performance in simulating procedure. In addition, GP and RSM models by a range of ($-1.57 \le ASRE \le 0.87$, error band: 2.44) and ($-1.51 \le ASRE \le 1.23$, error band: 2.74) can provide acceptable results to predict oil-based hybrid nanofluids' thermal conductivity. For efficient assessment of provided data-driven models, an attractive error analysis was carried out, which illustrated the cumulative frequency of percentage of ARE and ASRE for all datasets used in modeling (Fig. 8). The left side of Fig. 8 (continuous lines) displayed that in EKF-ANN, more than 90% of all datasets have the PRE% value equal to or less than 4.97 %, whereas 90 % of all data in RSM and GP was estimated with the PRE% value equal or less than 9.85% and 6.53%, respectively. This comparison inferred that EKF-ANN outperformed the GP and RSM models and RSM, despite the higher ASRE error band than GP had better modeling performance k_{nf}.

To further validate and evaluate the efficiency of the developed predictive model, eight existing thermal conductivity correlation extracted for oil-based hybrid nanofluid (i.e., Asadi et al.[54] and Soltani et al. [68]), provided for water&EG based hybrid nanofluids (Toghraie et al.[69], Harandi et al. [70], and Esfahani et al. [71]), and reported for mono nanofluid, were examined using several statistical criteria in Table 10. The comparison between the results of Table 10 confirmed that the EKF-ANN model is superior to the existing correlation in the estimation k_{nf}. Also, with respect to previous analyses, RSM and GP models as the second and third accurate approach have been yielded promising outcomes compared to considered correlation. According to the spider plot of performance metric in Fig. 9, Toghraie et al.[69] and Harandi et al. [70] 's equation in terms (R = 0.8033, RMSE = 0.0211 W/m.K, MAPE = 9.1402%, and KGE = 0.5476) and (R = 0.8025, RMSE = 0.0211W/m.K, MAPE = 9.1673%, and KGE = 0.5464), respectively led to more logical results than other relationships.

To assess the accuracy of the proposed EKF-ANN model in predicting different hybrid nano-fluids' thermal conductivity, the obtained values are compared with available measured data and some correlation equations. Here, three hybrid nanofluids, including TiO_2-SiC/Pure diathermic/oil [29], WO_3-MWCNTs/oil [124], and MgO-MWCNTs/Engine oil [55], are considered. For the first nanofluid, the variation of predicted thermal conductivity versus temperature is plotted in Fig. 10a. According to the measured data, it is clear that the EKF-ANN can predict the most accurate SiC/Pure diathermic/oil thermal conductivity values when compared with those of the developed data-driven approaches (i.e., the GP and RSM) and the correlation equation proposed by Toghraie et al. [69] (Fig. 10a). The best results of the EKF-ANN model are obtained in the range of 25^oC to 32^oC with relative error less than2%.

For different values of volume fraction and temperature, the thermal conductivity of Wo3-MWCNTs/oil nanofluid [124] compared to the experimental one is shown in Fig. 10b. For the high values of volume fraction (say 0.4%and 0.6%), the EKF-ANN model results have a perfect correlation with the measured values in different temperatures with a relative error less than 2.2%. The results associated with low volume fraction values (say 0.05%and 0.2%) have the maximum relative errors of 4.5% when compared with the measured data. These results indicate that the EKF-ANN model can predict the thermal conductivity of Wo3-MWCNTs/oil with acceptable accuracy under various conditions of volume fraction and temperature.

The variation of MgO-MWCNTs/Engine oil thermal conductivity versus volume fraction (in the range of 0.1%to 1.5%) at a constant temperature of 45^oC is shown in Fig. 10c. While the RSM model produces the more accurate results for volume fraction above 0.6%, the EKF-ANN model and Asadi et al.[55] have the most accurate among the considered models and correlations for volume fractions below 0.6%. Meanwhile, the maximum error observed in the EKF-ANN results is less than of 8%, which means that this model performed well in predicting the thermal conductivity of MgO-MWCNTs/Engine oil [55] with different volume fractions of nanoparticles. All of the results presented in Fig. 10 indicate that the proposed EKF-ANN model can predict nanofluids' thermal conductivity under different working conditions with acceptable accuracy. it is noteworthy that the relationship extracted from GP (Eq (26)) and RSM (Eq (27)) performing by the accuracy of R = 0.9465 and R = 0.9671, respectively, are listed in Table 11.

7. Sensitivity analysis

In this section, a sensitivity analysis is performed to determine the most sensitive parameters in the considered combination set in predicting hybrid nanofluids' thermal conductivity. The correlation coefficient and different errors and indices defined in the section are computed for each variable in the combination set and compared in Table 12. Based on the presented results, one can easily conclude that volume fraction is identified as the most sensitive parameter. It has the lowest value of the correlation coefficient (i.e., $R = 0.9066$) and the highest errors (i.e., $RMSE = 0.0135$ W/m.K, $MAPE = 0.0086$) among the considered parameters. After the volume fraction of nanoparticles, the nanoparticle average diameter and density earn second and third place in the list of the most sensitive variables. On the other hand, the temperature with $RMSE = 0.0079$W/m.K, $MAPE = 0.0048$, and $I_A = 0.9845$is known as the least influential variable in predicting the hybrid nanofluid thermal conductivity. Fig. 11 depicted the heat map of performance metrics for all situations of sensitivity analysis.

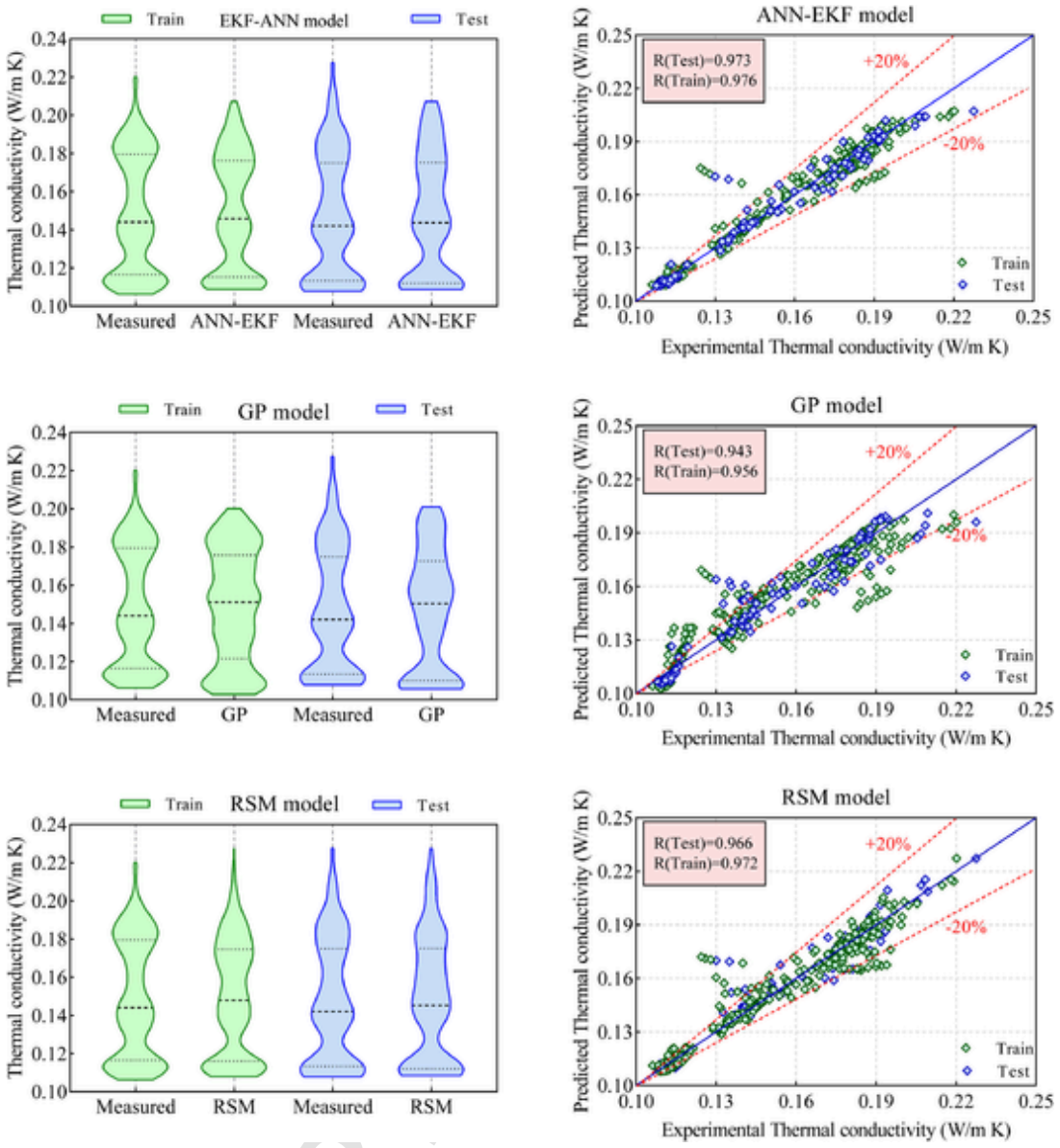

Fig. 6. the violin plots of distribution function (Left) and scatter plot (Right) of measured and predicted thermal conductivity of oil-based hybrid nanofluids

8. Outlier detection and applicability domain

Detection of outlier data and the domain of application is necessary for developed machine learning models. The leveraged approach is one of the most widely used and popular methods used in this field. In this method, the leverage index (H) is calculated using the following matrix [125][126]:

$$H = X\left(X^{T}X\right)X^{-1} \tag{28}$$

where X is a $n \times k$ matrix, where k is the number of model variables, and n is the number of samples [125]. The diagonal elements of the H matrix are known as the *hat*or leverage index. The standard residual (SR) is calculated from the following equation:

$$SR = \frac{(observed - model)}{StD\,(model)} \tag{29}$$

The standard residual (SR) is plotted against the *hat* to determine outlier data and model applicability domain. The warning value of the leverage index (H_*) is calculated using the following equation [127]:

$$H_* = \frac{3\,(k+1)}{n} \tag{30}$$

The diagram SR versus *hat* is known as the Williams diagram. Suppose most of the data are in the range of and . In that case, it indicates the appropriate application of the model in the mentioned range and therefore indicates the statistical validity of the developed model [127].

In the present study, to examine the outlier data and the application domain, the Williams diagram was plotted for the three machine learning models. Fig. 11 shows the Williams diagram for the three EKF-ANN, GP and SRM models. According to Fig. 12, all of the outputs of three ML models are in the range of $-3 < R < 3$ and $0 < H < H_*$, so they are statistically valid. Their application in estimating oil-based hybrid nanofluid thermal conductivity is highly reliable.

9. Conclusion and Remarks

In this study, a novel hybrid machine learning algorithm, extended Kalman filter integrated with freed-forward neural network (EKF-ANN) algorithm, is

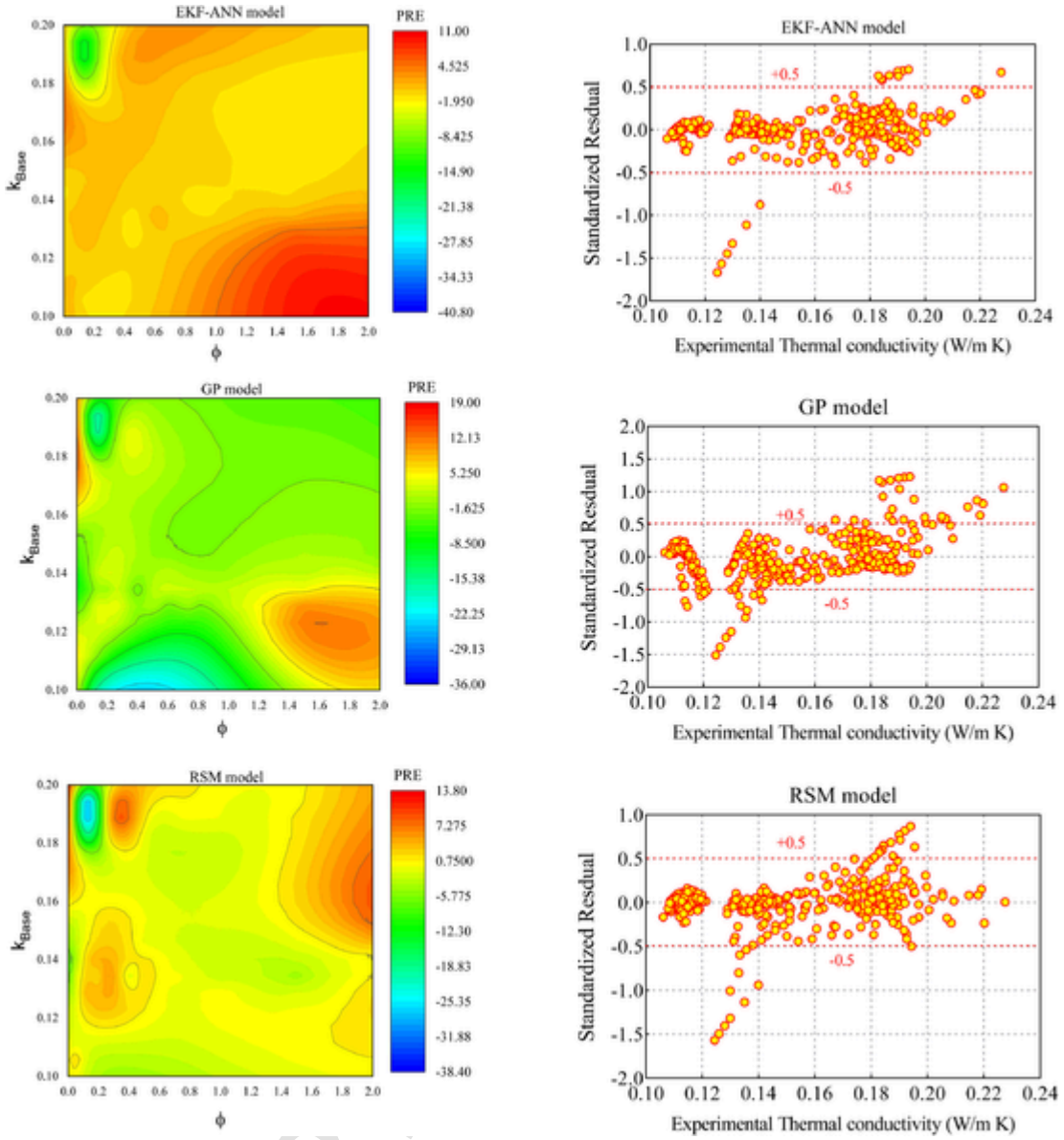

Fig. 7. The percentage of relative error contours (Left) and standardized residual error distribution (Right) for comparison of predictive performance data-driven models

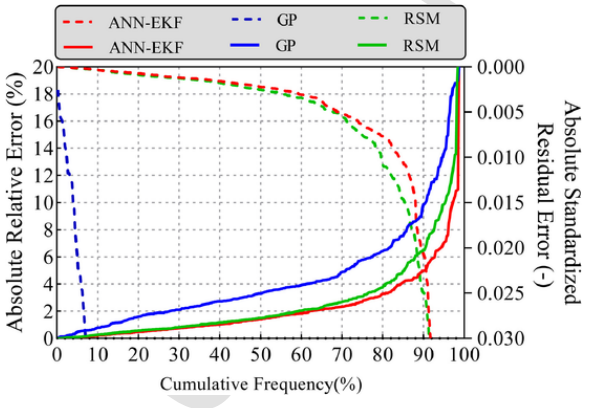

Fig. 8. Cumulative frequency of percentage of ARE and ASRE for all developed predictive models

used to provide an accurate prediction of oil-based nanofluids based on volume fraction (ϕ), temperature (T), the thermal conductivity of the base fluid (k_{Base}), mean diameter (D_{p1}andD_{p2}) and bulk density ($\rho_1$andρ_2) of nanoparticles as predictor features. Besides, the GP and RSM model were adopted to better validate of EKF-ANN approach. The outcomes of this research are presented as follows:

- An efficient feature selection, best subset regression analysis, was examined to achieve the best modeling results. The performed analysis indicated that the best input combination in terms of Mallow, Mameliya's prediction, and Akaike's information criteria included all the input variables.
- The results demonstrated that the EKF-ANN approach showed the most value of R = 0.9738, KGE = 0.9630, and IA = 0.9866. The lowest error metric RMSE = 0.0071W/m.K and MAPE = 2.4751%) is identified as the superior for estimation of thermal conductivity of oil-based hybrid nanofluids. Moreover, the RSM approach in terms of (R = 0.9671, RMSE = 0.0079 W/m.K, KGE = 0.9593 and MAPE = 2.9219%) outperformed the GP model (R = 0.9465, RMSE = 0.010 W/m.K, KGE = 0.9273 and MAPE = 4.6257%) and all existing empirical correlations.
- Efficiency assessment of the model using the error analysis demonstrated that the EKF-ANN approach by the minimum range $-1.67 \leq ASRE \leq 0.7$ had the best predictive performance compared to the GP and RSM models.

Table 10
the comparison of the predictive data-driven models' performance with the existing empirical-based correlations

Metrics	Pak and Cho [67]	Mintsa et al.[72]	Soltani et al.[68]	Asadi et al.[54]	Toghraie et al.[69]	Harandi et al. [70]	Esfahani et al.[71]	EKF-ANN
R	0.7580	0.7138	0.7285	0.5555	0.8033	0.8025	0.7759	0.9738
RMSE	0.0243	0.0272	0.0282	0.0345	0.0211	0.0211	0.0238	0.0071
MAPE	10.5948	11.6215	12.9285	22.6308	9.1402	9.1673	10.6162	2.4751
RAE	0.6296	0.6942	0.7582	1.0429	0.5412	0.5429	0.6294	0.1386
KGE	0.4729	0.4013	0.4033	0.0371	0.5476	0.5464	0.4835	0.9630
I_A	0.8291	0.7833	0.7762	0.5389	0.8776	0.8767	0.8351	0.9866

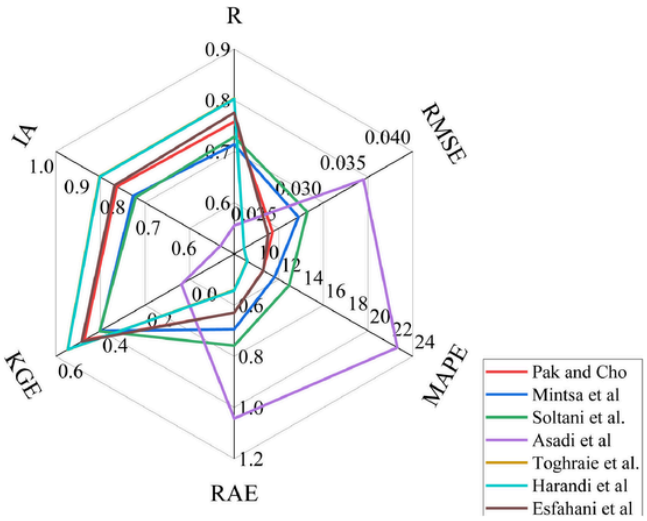

Fig. 9. The spider plot of metric performance for all existing correlation to predict the thermal conductivity of nanofluids

- The volume fraction was identified as the most influential input parameter in the simulation of oil-based hybrid nanofluids thermal conductivity.
- The leveraged approach demonstrated that all numbers of samples are located in the applicability domain. Three proposed data-driven models (three EKF-ANN, GP, and RSM) statistically are at a high level of reliability in estimating oil-based hybrid nanofluid thermal conductivity.

CRediT author statement

M. Jamei was responsible for Conceptualization, Methodology, Writing- Original draft preparation. **I. A. olumegbon, M. Karbasi, I. Ahamdianfar, and M. Mosharaf-Dehkordi** were responsible for formal analysis, validation, and data curation. **A. Asadi** was responsible reviewing and editing the manuscript and supervising the project.

Declaration of Competing Interest

The authors declare that they have no known competing financial interests or personal relationships that could have appeared to influence the work reported in this paper.

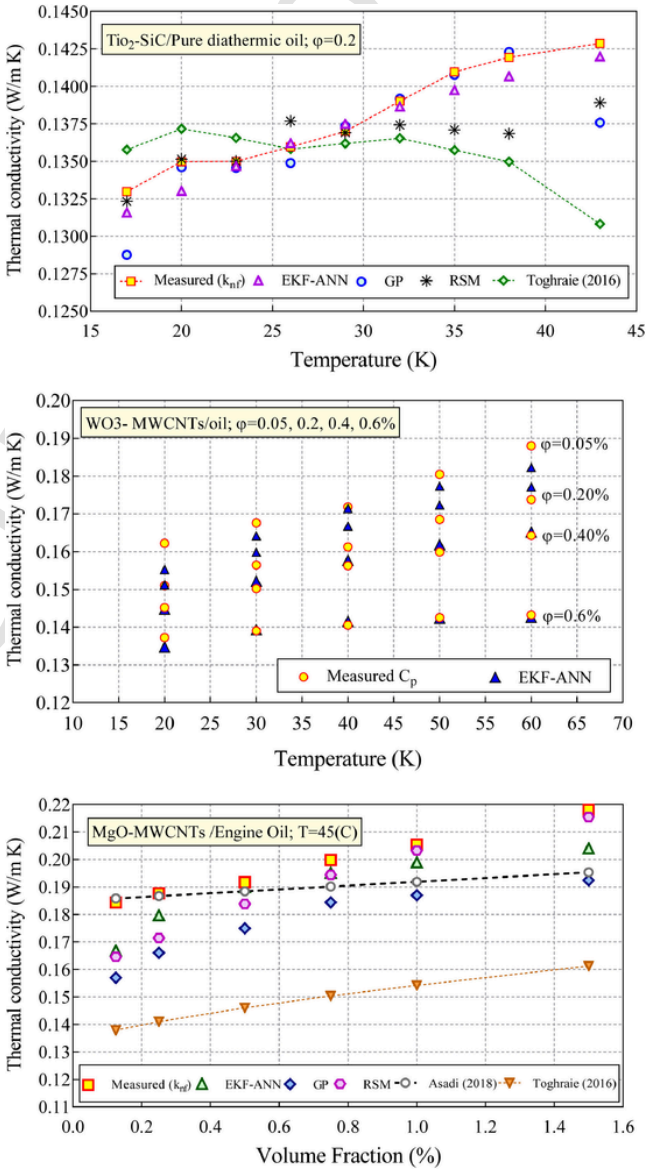

Fig. 10. Variation of thermal conductivity of (a): Tio2-SiC/Pure diathermic oil [29] (b): Wo3-MWCNTs/Oil [124] versus temperature (C) and (c) variation of thermal conductivity of MgO-MWCNTs/Engine oil [55] versus volume fraction (%) by using developed data-driven approaches and the existing correlation equations.

Table 11
The relationship extracted from the GP and RSM methods to estimate the thermal conductivity of oil-based hybrid nanofluids

Model	Formula	Equation
GP	$k_{nf} = \frac{0.1221(\phi+\rho_2+8.853k_{Base}-6.584)}{0.2896D_{p1}-\phi\rho_1+0.1169\phi T\rho_2} + 0.2062$	(26)
RSM	$k_{nf} = -0.7561 + 0.0538\phi - 0.0001T + 0.0080D_{P1} + 0.0125\rho_1 + 0.0588D_{P2} + 0.0228\rho_2 + 2.3999k_{Base} + 0.0005\phi T + 0.0004\phi D_{P1} + 0.0100\phi\rho_2 - 0.3476\phi k_{Base} - 0.0727D_{P1}k_{Base} - 0.2820\rho_1 k_{Base} - 0.0143\phi^2 + 0.0026{\rho_1}^2$	(27)

Table 12
The outcome of sensitivity analysis using RSM model

Metrics	All-ϕ	All-T	All-D_p	All-ρ	All-k_{Base}	All
R	0.9066	0.9695	0.9682	0.9701	0.9691	0.9720
RMSE	0.0135	0.0079	0.0082	0.0079	0.0080	0.0077
MAPE	0.0086	0.0048	0.0049	0.0049	0.0051	0.0045
E	0.3119	0.1725	0.1783	0.1783	0.1835	0.1623
RAE	5.6307	3.2045	3.2487	3.3405	3.3793	2.9722
KGE	0.8212	0.9387	0.9343	0.9389	0.9370	0.9422
IA	0.9486	0.9845	0.9836	0.9846	0.9841	0.9855
Rank	1	5	2	3	4	-

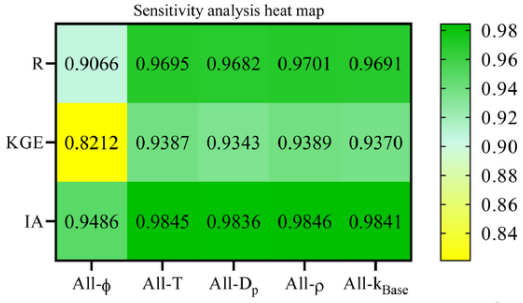

Fig. 11. The statistical parameters for all sensitivity analysis situations were obtained by the RSM model.

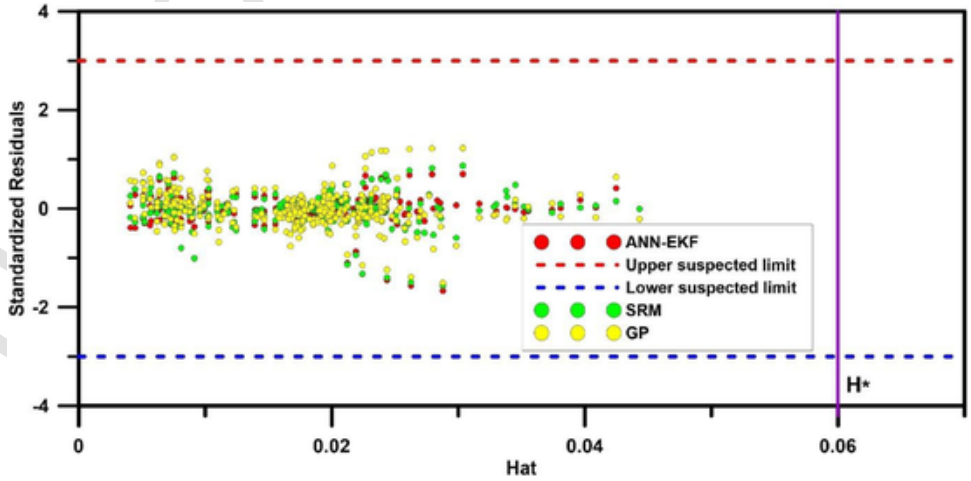

Fig. 12. Willliam's plot for measuring the applicability domain of EKF-ANN, GP, and SRM models

References

[1] S.U.S. Choi, S. Li, J.A. Eastman, Measuring thermal conductivity of fluids containing oxide nanoparticles, J. Heat Transfer. 121 (1999) 280–289, doi:10.1115/1.2825978.

[2] A. Asadi, I.M. Alarifi, Effects of ultrasonication time on stability, dynamic viscosity, and pumping power management of MWCNT-water nanofluid: an experimental study, Sci. Rep. 10 (2020) 15182, doi:10.1038/s41598-020-71978-9.

[3] A. Alshayji, A. Asadi, I.M. Alarifi, On the heat transfer effectiveness and pumping power assessment of a diamond-water nanofluid based on thermophysical properties: An experimental study, Powder Technol 373 (2020) 397–410, doi:10.1016/j.powtec.2020.06.068.

[4] N. Ali, J.A. Teixeira, A. Addali, Aluminium Nanofluids Stability: A Comparison between the Conventional Two-Step Fabrication Approach and the Controlled Sonication Bath Temperature Method, J. Nanomater. 2019 (2019), doi:10.1155/2019/3930572.

[5] S. Aberoumand, A. Jafarimoghaddam, Experimental study on synthesis, stability, thermal conductivity and viscosity of Cu–engine oil nanofluid, J. Taiwan Inst. Chem. Eng. 71 (2017) 315–322, doi:10.1016/J.JTICE.2016.12.035.

[6] Z. Lyu, A. Asadi, I.M. Alarifi, V. Ali, L.K. Foong, Thermal and Fluid Dynamics Performance of MWCNT-Water Nanofluid Based on Thermophysical Properties: An Experimental and Theoretical Study, Sci. Rep. 10 (2020) 5185, doi:10.1038/s41598-020-62143-3.

[7] A. Asadi, A guideline towards easing the decision-making process in selecting an effective nanofluid as a heat transfer fluid, Energy Convers. Manag. 175 (2018), doi:10.1016/j.enconman.2018.08.101.

[8] S.S. Soleimani, S. Jahandari, S. Aberoumand, A. Rahmani, A. Shokrgozar, Cu/Oil nanofluids flow over a semi-infinite plate accounting an experimental model, Heat Transf 49 (2020) 1338–1354, doi:10.1002/htj.21664.

[9] A. Jafarimoghaddam, S. Aberoumand, K. Javaherdeh, A.A.A. Arani, R. Jafarimoghaddam, Al/oil nanofluids inside annular tube: an experimental study on convective heat transfer and pressure drop, Heat Mass Transf. Und Stoffuebertragung. 54 (2018) 1053–1067, doi:10.1007/s00231-017-2199-9.

[10] A. Asadi, F. Pourfattah, I. Miklós Szilágyi, M. Afrand, G. Żyła, H. Seon Ahn, S. Wongwises, H. Minh Nguyen, A. Arabkoohsar, O. Mahian, Effect of sonication characteristics on stability, thermophysical properties, and heat transfer of nanofluids: A comprehensive review, Ultrason. Sonochem. 58 (2019) 104701, doi:10.1016/J.ULTSONCH.2019.104701.

[11] S. Aberoumand, P. Woodfield, B. Shabani, D.V. Dao, Advances in electrode and electrolyte improvements in vanadium redox flow batteries with a focus on the nanofluidic electrolyte approach, Phys. Rep. (2020), doi:10.1016/j.physrep.2020.08.001.

[12] Z. Said, A.A. Hachicha, S. Aberoumand, B.A.A. Yousef, E.T. Sayed, E. Bellos, Recent advances on nanofluids for low to medium temperature solar collectors: energy, exergy, economic analysis and environmental impact, Prog. Energy Combust. Sci. 84 (2021) 100898, doi:10.1016/j.pecs.2020.100898.

[13] N. Ali, J.A. Teixeira, A. Addali, A Review on Nanofluids: Fabrication, Stability, and Thermophysical Properties, J. Nanomater. 2018 (2018), doi:10.1155/2018/6978130.

[14] S. Almurtaji, N. Ali, J.A. Teixeira, A. Addali, On the Role of Nanofluids in Thermal-hydraulic Performance of Heat Exchangers—A Review, Nanomaterials 10 (2020) 734, doi:10.3390/nano10040734.

[15] A. Alsayegh, N. Ali, Gas Turbine Intercoolers: Introducing Nanofluids—A Mini-Review, Processes 8 (2020) 1572, doi:10.3390/pr8121572.

[16] A. Asadi, S. Aberoumand, A. Moradikazerouni, F. Pourfattah, G. Żyła, P. Estellé, O. Mahian, S. Wongwises, H.M. Nguyen, A. Arabkoohsar, Recent advances in preparation methods and thermophysical properties of oil-based nanofluids: A state-of-the-art review, Powder Technol (2019), doi:10.1016/J.POWTEC.2019.04.054.

[17] J. Sarkar, P. Ghosh, A. Adil, A review on hybrid nanofluids: Recent research, development and applications, Renew. Sustain. Energy Rev. 43 (2015) 164–177, doi:10.1016/j.rser.2014.11.023.

[18] H. Li, C.S. Ha, I. Kim, Fabrication of carbon nanotube/SiO 2 and carbon nanotube/SiO 2/AG nanoparticles hybrids by using plasma treatment, Nanoscale Res. Lett. 4 (2009) 1384–1388, doi:10.1007/s11671-009-9409-4.

[19] M.A. Nazari, R. Ghasempour, M.H. Ahmadi, G. Heydarian, M.B. Shafii, Experimental investigation of graphene oxide nanofluid on heat transfer enhancement of pulsating heat pipe, Int. Commun. Heat Mass Transf. 91 (2018) 90–94, doi:10.1016/j.icheatmasstransfer.2017.12.006.

[20] M. Alhuyi Nazari, M.H. Ahmadi, R. Ghasempour, M.B. Shafii, How to improve the thermal performance of pulsating heat pipes: A review on working fluid, Renew. Sustain. Energy Rev. 91 (2018) 630–638, doi:10.1016/j.rser.2018.04.042.

[21] E. Bellos, C. Tzivanidis, A review of concentrating solar thermal collectors with and without nanofluids, J. Therm. Anal. Calorim. 135 (2019) 763–786, doi:10.1007/s10973-018-7183-1.

[22] O. Mahian, L. Kolsi, M. Amani, P. Estellé, G. Ahmadi, C. Kleinstreuer, J.S. Marshall, M. Siavashi, R.A. Taylor, H. Niazmand, S. Wongwises, T. Hayat, A. Kolanjiyil, A. Kasaeian, I. Pop, Recent advances in modeling and simulation of nanofluid flows-Part I: Fundamentals and theory, Phys. Rep. 790 (2019) 1–48, doi:10.1016/j.physrep.2018.11.004.

[23] M. Baghbanzadeh, A. Rashidi, D. Rashtchian, R. Lotfi, A. Amrollahi, Synthesis of spherical silica/multiwall carbon nanotubes hybrid nanostructures and investigation of thermal conductivity of related nanofluids, Thermochim. Acta. 549 (2012) 87–94, doi:10.1016/j.tca.2012.09.006.

[24] M. Baghbanzadeh, A. Rashidi, A.H. Soleimanisalim, D. Rashtchian, Investigating the rheological properties of nanofluids of water/hybrid nanostructure of spherical silica/MWCNT, Thermochim. Acta. 578 (2014) 53–59, doi:10.1016/j.tca.2014.01.004.

[27] D. Madhesh, R. Parameshwaran, S. Kalaiselvam, Experimental investigation on convective heat transfer and rheological characteristics of Cu-TiO2 hybrid nanofluids, Exp. Therm. Fluid Sci. 52 (2014) 104–115, doi:10.1016/j.expthermflusci.2013.08.026.

[28] M.U. Sajid, H.M. Ali, Thermal conductivity of hybrid nanofluids: A critical review, Int. J. Heat Mass Transf. 126 (2018) 211–234, doi:10.1016/j.ijheatmasstransfer.2018.05.021.

[29] B. Wei, C. Zou, X. Yuan, X. Li, Thermo-physical property evaluation of diathermic oil based hybrid nanofluids for heat transfer applications, Int. J. Heat Mass Transf. 107 (2017) 281–287, doi:10.1016/j.ijheatmasstransfer.2016.11.044.

[30] M. Hemmat Esfe, S. Saedodin, M. Biglari, H. Rostamian, Experimental investigation of thermal conductivity of CNTs-Al2O3/water: A statistical approach, Int. Commun. Heat Mass Transf. 69 (2015) 29–33, doi:10.1016/j.icheatmasstransfer.2015.10.005.

[31] M. Farbod, A. Ahangarpour, Improved thermal conductivity of Ag decorated carbon nanotubes water based nanofluids, Phys. Lett. Sect. A Gen. At. Solid State Phys. 380 (2016) 4044–4048, doi:10.1016/j.physleta.2016.10.014.

[32] R.N. Ramachandran, K. Ganesan, L.G. Asirvatham, The role of hybrid nanofluids in improving the thermal characteristics of screen mesh cylindrical heat pipes, Therm. Sci. 20 (2016) 2027–2035, doi:10.2298/TSCI150710006R.

[33] S. Suresh, K.P. Venkitaraj, P. Selvakumar, M. Chandrasekar, Synthesis of Al2O3-Cu/water hybrid nanofluids using two step method and its thermo physical properties, Colloids Surfaces A Physicochem. Eng. Asp. 388 (2011) 41–48, doi:10.1016/j.colsurfa.2011.08.005.

[34] S. Jana, A. Salehi-Khojin, W.H. Zhong, Enhancement of fluid thermal conductivity by the addition of single and hybrid nano-additives, Thermochim. Acta. 462 (2007) 45–55, doi:10.1016/j.tca.2007.06.009.

[35] S.M. Abbasi, A. Rashidi, A. Nemati, K. Arzani, The effect of functionalisation method on the stability and the thermal conductivity of nanofluid hybrids of carbon nanotubes/gamma alumina, Ceram. Int. 39 (2013) 3885–3891, doi:10.1016/j.ceramint.2012.10.232.

[36] M.H. Ahmadi, A. Mirlohi, M. Alhuyi Nazari, R. Ghasempour, A review of thermal conductivity of various nanofluids, J. Mol. Liq. 265 (2018) 181–188, doi:10.1016/j.molliq.2018.05.124.

[37] A.A. Abdullah, S.A. Althobaiti, K.A. Lindsay, Marangoni convection in water–alumina nanofluids: Dependence on the nanoparticle size, Eur. J. Mech. B/Fluids. 67 (2018) 259–268, doi:10.1016/j.euromechflu.2017.09.015.

[38] L. Chen, H. Xie, Silicon oil based multiwalled carbon nanotubes nanofluid with optimized thermal conductivity enhancement, Colloids Surfaces A Physicochem. Eng. Asp. 352 (2009) 136–140, doi:10.1016/j.colsurfa.2009.10.015.

[39] W. Yu, H. Xie, L. Chen, Y. Li, Enhancement of thermal conductivity of kerosene-based Fe3O4 nanofluids prepared via phase-transfer method, Colloids Surfaces A Physicochem. Eng. Asp. 355 (2010) 109–113, doi:10.1016/j.colsurfa.2009.11.044.

[40] M.S. Kumar, V. Vasu, A.V. Gopal, Thermal conductivity and rheological studies for Cu–Zn hybrid nanofluids with various basefluids, J. Taiwan Inst. Chem. Eng. 66 (2016) 321–327, doi:10.1016/j.jtice.2016.05.033.

[41] W. Aftab, X. Huang, R. Zou, The application of carbon materials in latent heat thermal energy storage (LHTES), Therm. Transp. Carbon-Based Nanomater, Elsevier, 2017, pp. 243–265.

[42] W. Aftab, X. Huang, W. Wu, Z. Liang, A. Mahmood, R. Zou, Nanoconfined phase change materials for thermal energy applications, Energy Environ. Sci. 11 (2018) 1392–1424.

[43] Q. Wang, B. Liu, Z. Wang, Investigation of heat transfer mechanisms among particles in horizontal rotary retorts, Powder Technol 367 (2020) 82–96.

[44] B. Wang, Z. Song, L. Sun, A review, Comparison of multi-air-pollutant removal by advanced oxidation processes–Industrial implementation for catalytic oxidation processes, Chem. Eng. J. (2020) 128136.

[45] S. Chen, M.K. Hassanzadeh-Aghdam, R. Ansari, An analytical model for elastic modulus calculation of SiC whisker-reinforced hybrid metal matrix nanocomposite containing SiC nanoparticles, J. Alloys Compd. 767 (2018) 632–641.

[46] T.T. Baby, S. Ramaprabhu, Experimental investigation of the thermal transport properties of a carbon nanohybrid dispersed nanofluid, Nanoscale 3 (2011) 2208–2214, doi:10.1039/c0nr01024c.

[47] T.T. Baby, S. Ramaprabhu, Synthesis and nanofluid application of silver nanoparticles decorated graphene, J. Mater. Chem. 21 (2011) 9702–9709, doi:10.1039/c0jm04106h.

[48] L. Syam Sundar, M.K. Singh, M.C. Ferro, A.C.M. Sousa, Experimental investigation of the thermal transport properties of graphene oxide/Co3O4 hybrid nanofluids, Int. Commun. Heat Mass Transf. 84 (2017) 1–10, doi:10.1016/j.icheatmasstransfer.2017.03.001.

[49] L.S. Sundar, G.O. Irurueta, E. Venkata Ramana, M.K. Singh, A.C.M. Sousa, Thermal conductivity and viscosity of hybrid nanfluids prepared with magnetic nanodiamond-cobalt oxide (ND-Co3O4) nanocomposite, Case Stud, Therm. Eng. 7 (2016) 66–77, doi:10.1016/j.csite.2016.03.001.

[50] L.S. Sundar, E. Venkata Ramana, M.P.F. Graça, M.K. Singh, A.C.M. Sousa, Nanodiamond-Fe3O4 nanofluids: Preparation and measurement of viscosity, electrical and thermal conductivities, Int. Commun. Heat Mass Transf. 73 (2016) 62–74, doi:10.1016/j.icheatmasstransfer.2016.02.013.

[51] M.J. Nine, M. Batmunkh, J.H. Kim, H.S. Chung, H.M. Jeong, Investigation of Al 2O 3-MWCNTs hybrid dispersion in water and their thermal characterization, J. Nanosci. Nanotechnol. 12 (2012) 4553–4559, doi:10.1166/jnn.2012.6193.

[52] M. Chopkar, S. Kumar, D.R. Bhandari, P.K. Das, I. Manna, Development and characterization of Al2Cu and Ag2Al nanoparticle dispersed water and ethylene glycol based nanofluid, Mater. Sci. Eng. B Solid-State Mater. Adv. Technol. 139 (2007) 141–148, doi:10.1016/j.mseb.2007.01.048.

[53] G. Paul, J. Philip, B. Raj, P.K. Das, I. Manna, Synthesis, characterization, and thermal property measurement of nano-Al95Zn05 dispersed nanofluid prepared

[55] M. Asadi, A. Asadi, S. Aberoumand, An experimental and theoretical investigation on the effects of adding hybrid nanoparticles on heat transfer efficiency and pumping power of an oil-based nanofluid as a coolant flui, Int. J. Refrig. (2018), doi:10.1016/j.ijrefrig.2018.03.014.
[56] A. Asadi, M. Asadi, A. Rezaniakolaei, L.A. Rosendahl, S. Wongwises, An experimental and theoretical investigation on heat transfer capability of Mg (OH) 2 /MWCNT-engine oil hybrid nano-lubricant adopted as a coolant and lubricant fluid, Appl. Therm. Eng. 129 (2018) 577–586, doi:10.1016/j.applthermaleng.2017.10.074.
[57] S.K. Mechiri, V. Vasu, A. Venu Gopal, Investigation of thermal conductivity and rheological properties of vegetable oil based hybrid nanofluids containing Cu–Zn hybrid nanoparticles, Exp. Heat Transf. 30 (2017) 205–217, doi:10.1080/08916152.2016.1233147.
[58] S.H. Qing, W. Rashmi, M. Khalid, T.C.S.M. Gupta, M. Nabipoor, M.T. Hajibeigy, Thermal conductivity and electrical properties of Hybrid SiO2-graphene naphthenic mineral oil nanofluid as potential transformer oil, Mater. Res. Express. 4 (2017) 015504, doi:10.1088/2053-1591/aa550e.
[59] S.S. Botha, P. Ndungu, B.J. Bladergroen, Physicochemical properties of oil-based nanofluids containing hybrid structures of silver nanoparticles supported on silica, Ind. Eng. Chem. Res. 50 (2011) 3071–3077, doi:10.1021/ie101088x.
[60] S. Aberoumand, A. Jafarimoghaddam, Tungsten (III) oxide (WO3) – Silver/transformer oil hybrid nanofluid: Preparation, stability, thermal conductivity and dielectric strength, Alexandria Eng. J. 57 (2018) 169–174, doi:10.1016/j.aej.2016.11.003.
[61] A Treatise on Electricity and Magnetism - James Clerk Maxwell - Oxford University Press, (n.d.).
[62] R.L. Hamilton, Thermal conductivity of heterogeneous two-component systems, Ind. Eng. Chem. Fundam. 1 (1962) 187–191, doi:10.1021/i160003a005.
[63] W. Yu, S.U.S. Choi, The role of interfacial layers in the enhanced thermal conductivity of nanofluids: A renovated Maxwell model, J. Nanoparticle Res. 5 (2003) 167–171, doi:10.1023/A:1024438603801.
[64] P. Bhattacharya, S.K. Saha, A. Yadav, P.E. Phelan, R.S. Prasher, Brownian dynamics simulation to determine the effective thermal conductivity of nanofluids, J. Appl. Phys. 95 (2004) 6492–6494, doi:10.1063/1.1736319.
[65] M. Hamid, M. Usman, Z.H. Khan, R.U. Haq, W. Wang, Heat transfer and flow analysis of Casson fluid enclosed in a partially heated trapezoidal cavity, Int. Commun. Heat Mass Transf. 108 (2019) 104284.
[66] M. Hamid, M. Usman, Z.H. Khan, R.U. Haq, W. Wang, Numerical study of unsteady MHD flow of Williamson nanofluid in a permeable channel with heat source/sink and thermal radiation, Eur. Phys. J. Plus. 133 (2018) 1–12.
[67] B.C. Pak, Y.I. Cho, Hydrodynamic and heat transfer study of dispersed fluids with submicron metallic oxide particles, Exp. Heat Transf. 11 (1998) 151–170, doi:10.1080/08916159808946559.
[68] F. Soltani, D. Toghraie, A. Karimipour, Experimental measurements of thermal conductivity of engine oil-based hybrid and mono nanofluids with tungsten oxide (WO3) and MWCNTs inclusions, Powder Technol (2020), doi:10.1016/j.powtec.2020.05.059.
[69] D. Toghraie, V.A. Chaharsoghi, M. Afrand, Measurement of thermal conductivity of ZnO–TiO2/EG hybrid nanofluid: Effects of temperature and nanoparticles concentration, J. Therm. Anal. Calorim. 125 (2016) 527–535, doi:10.1007/s10973-016-5436-4.
[70] S. Sarboolookzadeh Harandi, A. Karimipour, M. Afrand, M. Akbari, A. D'Orazio, An experimental study on thermal conductivity of F-MWCNTs-Fe3O4/EG hybrid nanofluid: Effects of temperature and concentration, Int. Commun. Heat Mass Transf. 76 (2016) 171–177, doi:10.1016/j.icheatmasstransfer.2016.05.029.
[71] N.N. Esfahani, D. Toghraie, M. Afrand, A new correlation for predicting the thermal conductivity of ZnO–Ag (50%–50%)/water hybrid nanofluid: An experimental study, Powder Technol 323 (2018) 367–373, doi:10.1016/j.powtec.2017.10.025.
[72] H.A. Mintsa, G. Roy, C.T. Nguyen, D. Doucet, New temperature dependent thermal conductivity data for water-based nanofluids, Int. J. Therm. Sci. 48 (2009) 363–371, doi:10.1016/j.ijthermalsci.2008.03.009.
[73] M.H. Ahmadi, B. Mohseni-Gharyehsafa, M. Farzaneh-Gord, R.D. Jilte, R. Kumar, K. Chau, Applicability of connectionist methods to predict dynamic viscosity of silver/water nanofluid by using ANN-MLP, MARS and MPR algorithms, Eng. Appl. Comput. Fluid Mech. 13 (2019) 220–228, doi:10.1080/19942060.2019.1571442.
[74] M.K. Meybodi, S. Naseri, A. Shokrollahi, A. Daryasafar, Prediction of viscosity of water-based Al2O3, TiO2, SiO2, and CuO nanofluids using a reliable approach, Chemom. Intell. Lab. Syst. 149 (2015) 60–69, doi:10.1016/j.chemolab.2015.10.001.
[75] F. Yousefi, H. Karimi, M.M. Papari, Modeling viscosity of nanofluids using diffusional neural networks, J. Mol. Liq. 175 (2012) 85–90, doi:10.1016/j.molliq.2012.08.015.
[76] M. Jamei, I. Ahmadianfar, A rigorous model for prediction of viscosity of oil-based hybrid nanofluids, Phys. A Stat. Mech. Its Appl. (2020) 124827.
[77] M. Gholizadeh, M. Jamei, I. Ahmadianfar, R. Pourrajab, Prediction of nanofluids viscosity using random forest (RF) approach, Chemom. Intell. Lab. Syst. 201 (2020) 104010, doi:10.1016/j.chemolab.2020.104010.
[78] I.O. Alade, M.A.A. Rahman, T.A. Saleh, An approach to predict the isobaric specific heat capacity of nitrides/ethylene glycol-based nanofluids using support vector regression, J. Energy Storage. 29 (2020) 101313, doi:10.1016/j.est.2020.101313.
[79] I.O. Alade, M.A. Abd Rahman, T.A. Saleh, Modeling and prediction of the specific heat capacity of Al2 O3/water nanofluids using hybrid genetic algorithm/support vector regression model, Nano-Structures & Nano-Objects 17 (2019) 103–111, doi:10.1016/J.NANOSO.2018.12.001.
[80] I.O. Alade, M.A. Abd Rahman, T.A. Saleh, Predicting the specific heat capacity of alumina/ethylene glycol nanofluids using support vector regression model
[83] R. Pourrajab, I. Ahmadianfar, M. Jamei, M. Behbahani, A meticulous intelligent approach to predict thermal conductivity ratio of hybrid nanofluids for heat transfer applications, J. Therm. Anal. Calorim. (2020) 1–18.
[84] I.A., M.B. Ali Naseri, Mehdi Jamei, Nanofluids Thermal Conductivity prediction applying a Novel Hybrid Data-Driven Model Validated using Monte Carlo based Sensitivity Analysis, Eng. Comput. (2020), doi:10.1007/s00366-020-01163-z.
[85] I. Wole-Osho, E.C. Okonkwo, H. Adun, D. Kavaz, S. Abbasoglu, An intelligent approach to predicting the effect of nanoparticle mixture ratio, concentration and temperature on thermal conductivity of hybrid nanofluids, J. Therm. Anal. Calorim. (2020) 1–18.
[86] H. Adun, I. Wole-Osho, E.C. Okonkwo, O. Bamisile, M. Dagbasi, S. Abbasoglu, A neural network-based predictive model for the thermal conductivity of hybrid nanofluids, Int. Commun. Heat Mass Transf. 119 (2020) 104930.
[87] M. Jamei, I. Ahmadianfar, I.A. Olumegbon, A. Asadi, M. Karbasi, Z. Said, M. Sharifpur, J.P. Meyer, On the specific heat capacity estimation of metal oxide-based nanofluid for energy perspective – A comprehensive assessment of data analysis techniques, Int. Commun. Heat Mass Transf. (2021).
[88] M.A. Ariana, B. Vaferi, G. Karimi, Prediction of thermal conductivity of alumina water-based nanofluids by artificial neural networks, Powder Technol 278 (2015) 1–10, doi:10.1016/j.powtec.2015.03.005.
[89] I.O. Alade, T.A. Oyehan, I.K. Popoola, S.O. Olatunji, A. Bagudu, Modeling thermal conductivity enhancement of metal and metallic oxide nanofluids using support vector regression, Adv. Powder Technol. 29 (2018) 157–167, doi:10.1016/j.apt.2017.10.023.
[90] H.H. Balla, S. Abdullah, W.M.F. Wanmahmood, M. Abdul Razzaq, R. Zulkifli, K. Sopian, Modelling and measuring the thermal conductivity of multi-metallic Zn/Cu nanofluid, Res. Chem. Intermed. 39 (2013) 2801–2815, doi:10.1007/s11164-012-0799-z.
[91] S.H. Rostamian, M. Biglari, S. Saedodin, M. Hemmat Esfe, An inspection of thermal conductivity of CuO-SWCNTs hybrid nanofluid versus temperature and concentration using experimental data, ANN modeling and new correlation, J. Mol. Liq. 231 (2017) 364–369, doi:10.1016/j.molliq.2017.02.015.
[92] M. Vafaei, M. Afrand, N. Sina, R. Kalbasi, F. Sourani, H. Teimouri, Evaluation of thermal conductivity of MgO-MWCNTs/EG hybrid nanofluids based on experimental data by selecting optimal artificial neural networks, Phys. E Low-Dimensional Syst. Nanostructures. 85 (2017) 90–96, doi:10.1016/j.physe.2016.08.020.
[93] M. Hemmat Esfe, A.A. Abbasian Arani, M. Firouzi, Empirical study and model development of thermal conductivity improvement and assessment of cost and sensitivity of EG-water based SWCNT-ZnO (30%:70%) hybrid nanofluid, J. Mol. Liq. 244 (2017) 252–261, doi:10.1016/j.molliq.2017.08.087.
[94] M. Hemmat Esfe, S. Esfandeh, S. Saedodin, H. Rostamian, Experimental evaluation, sensitivity analyzation and ANN modeling of thermal conductivity of ZnO-MWCNT/EG-water hybrid nanofluid for engineering applications, Appl. Therm. Eng. 125 (2017) 673–685, doi:10.1016/j.applthermaleng.2017.06.077.
[95] M.H. Esfe, M. Rejvani, R. Karimpour, A.A. Abbasian Arani, Estimation of thermal conductivity of ethylene glycol-based nanofluid with hybrid suspensions of SWCNT–Al2O3 nanoparticles by correlation and ANN methods using experimental data, J. Therm. Anal. Calorim. 128 (2017) 1359–1371, doi:10.1007/s10973-016-6002-9.
[96] M. Hemmat Esfe, S. Esfandeh, M. Rejvani, Modeling of thermal conductivity of MWCNT-SiO2(30:70%)/EG hybrid nanofluid, sensitivity analyzing and cost performance for industrial applications: An experimental based study, J. Therm. Anal. Calorim. 131 (2018) 1437–1447, doi:10.1007/s10973-017-6680-y.
[97] A. Shahsavar, M. Bahiraei, Experimental investigation and modeling of thermal conductivity and viscosity for non-Newtonian hybrid nanofluid containing coated CNT/Fe3O4 nanoparticles, Powder Technol 318 (2017) 441–450, doi:10.1016/j.powtec.2017.06.023.
[98] M.H. Esfe, A. Alirezaie, M. Rejvani, An applicable study on the thermal conductivity of SWCNT-MgO hybrid nanofluid and price-performance analysis for energy management, 111 (2017) 1202–1210.
[99] S. Kannaiyan, C. Boobalan, F.C. Nagarajan, S. Sivaraman, Modeling of thermal conductivity and density of alumina/silica in water hybrid nanocolloid by the application of Artificial Neural Networks, Chinese J. Chem. Eng. 27 (2019) 726–736, doi:10.1016/j.cjche.2018.07.018.
[100] M. Hemmat Esfe, A.A. Abbasian Arani, R. Shafiei Badi, M. Rejvani, M.H. Esfe, A. Akbar, A. Arani, R.S. Badi, M. Rejvani, ANN modeling, cost performance and sensitivity analyzing of thermal conductivity of DWCNT–SiO2/EG hybrid nanofluid for higher heat transfer: An experimental study, J. Therm. Anal. Calorim. 131 (2018) 2381–2393, doi:10.1007/s10973-017-6744-z.
[101] M. Usman, M. Hamid, T. Zubair, R.U. Haq, W. Wang, Cu-Al2O3/Water hybrid nanofluid through a permeable surface in the presence of nonlinear radiation and variable thermal conductivity via LSM, Int. J. Heat Mass Transf. 126 (2018) 1347–1356.
[102] B. Wei, C. Zou, X. Yuan, X. Li, International Journal of Heat and Mass Transfer Thermo-physical property evaluation of diathermic oil based hybrid nanofluids for heat transfer applications, Int. J. Heat Mass Transf. 107 (2017) 281–287, doi:10.1016/j.ijheatmasstransfer.2016.11.044.
[103] A. Ghaffarkhah, M. Afrand, M. Talebkeikhah, A.A. Sehat, M.K. Moraveji, F. Talebkeikhah, M. Arjmand, On evaluation of thermophysical properties of transformer oil-based nanofluids: a comprehensive modeling and experimental study, J. Mol. Liq. 300 (2020) 112249.
[104] D. Geroge, P. Mallery, SPSS for windows step by step: A simple guide and reference, 2003.
[105] N.H. Nie, D.H. Bent, C.H. Hull, SPSS: Statistical package for the social sciences, McGraw-Hill, New York, 1975.
[106] S.S. Shapiro, M.B. Wilk, An analysis of variance test for normality (complete samples), Biometrika 52 (1965) 591–611.
[107] M. Jamei, I. Ahmadianfar, Prediction of scour depth at piers with debris accumulation effects using linear genetic programming, Mar. Georesources Geotechnol. 38 (2020) 468–479.

[109] M. Kobayashi, S. Sakata, Mallows' Cp criterion and unbiasedness of model selection, J. Econom. 45 (1990) 385–395.
[110] H. Akaike, A new look at the statistical model identification, IEEE Trans. Automat. Contr. 19 (1974) 716–723.
[111] G. Claeskens, N.L. Hjort, Model selection and model averaging, Cambridge Books, 2008.
[112] S. Haykin, N. Network, A comprehensive foundation, Neural Networks 2 (2004) 41.
[113] S. Araghinejad, Data-driven modeling: using MATLAB® in water resources and environmental engineering, Springer Science & Business Media, 2013.
[114] G. Welch, G. Bishop, An introduction to the Kalman filter, 1995.
[115] C.K. Chui, G. Chen, Extended Kalman filter and system identification, Kalman Filter, Springer, 2017, pp. 115–137.
[116] Z. Chen, S. Qiu, M.A. Masrur, Y.L. Murphey, Battery state of charge estimation based on a combined model of Extended Kalman Filter and neural networks, 2011 Int. Jt. Conf. Neural Networks, IEEE, 2011, pp. 2156–2163.
[117] L. Zhang, P.B. Luh, Neural network-based market clearing price prediction and confidence interval estimation with an improved extended Kalman filter method, IEEE Trans. Power Syst. 20 (2005) 59–66.
[118] X. Wu, Y. Wang, Extended and Unscented Kalman filtering based feedforward neural networks for time series prediction, Appl. Math. Model. 36 (2012) 1123–1131.
[119] Z. Darojah, E.S. Ningrum, The extended Kalman filter algorithm for improving neural network performance in voice recognition classification, 2016 Int. Semin. Intell. Technol. Its Appl., IEEE, 2016, pp. 225–230.
[120] I. Rivals, L. Personnaz, A recursive algorithm based on the extended Kalman filter for the training of feedforward neural models, Neurocomputing 20 (1998) 279–294, doi:10.1016/S0925-2312(98)00021-6.
[121] K.A.M. Said, M.A.M. Amin, Overview on the response surface methodology (RSM) in extraction processes, J. Appl. Sci. Process Eng. 2 (2015).
[122] C.J. Willmott, Some Comments on the Evaluation of Model Performance, American Meteorological Society, 1982 (1982)063<1309:SCOTEO>2.0.CO;2, doi:10.1175/1520-0477.
[123] H.V Gupta, H. Kling, K.K. Yilmaz, G.F. Martinez, Decomposition of the mean squared error and NSE performance criteria: Implications for improving hydrological modelling, J. Hydrol. 377 (2009) 80–91.
[124] F. Soltani, D. Toghraie, A. Karimipour, Experimental measurements of thermal conductivity of engine oil-based hybrid and mono nanofluids with tungsten oxide (WO3) and MWCNTs inclusions, Powder Technol (2020), doi:10.1016/j.powtec.2020.05.059.
[125] P.J. Rousseeuw, A.M. Leroy, Robust regression and outlier detection, John wiley & sons, 2005.
[126] F. Gharagheizi, A. Eslamimanesh, M. Sattari, B. Tirandazi, A.H. Mohammadi, D. Richon, Evaluation of thermal conductivity of gases at atmospheric pressure through a corresponding states method, Ind. Eng. Chem. Res. 51 (2012) 3844–3849.
[127] I. Rehamnia, B. Benlaoukli, M. Jamei, M. Karbasi, Anurag Malikd, Simulation of Seepage Flow through Embankment Dam by Using a novel Extended Kalman Filter based neural network Paradigm: Case Study of Fontaine Gazelles Dam, Algeria, Measurement (2021).